NASA Contractor Report 159101

NASA-CR-159101
19790023180

COMPARATIVE EVALUATION OF WOVEN GRAPHITE-EPOXY COMPOSITES

S. Hanagud, A. Tayebi, R. G. Clinton, Jr.,
and B. M. Nayak

GEORGIA INSTITUTE OF TECHNOLOGY
Atlanta, Georgia 30332

NASA Grant NSG-1352
July 1979

National Aeronautics and
Space Administration

Langley Research Center
Hampton, Virginia 23665

Final Report
E-16-604

COMPARATIVE EVALUATION OF WOVEN GRAPHITE-EPOXY COMPOSITES

Principal Investigators: S. Hanagud (A.E.)
A. Tayebi (Text. Eng.)

Research Assistants: R. G. Clinton Jr.
B. M. Nayak

ABSTRACT

A comparative evaluation of some of the mechanical properties of woven graphite-epoxy composites have been discussed in this report. In particular the types of weaves and the resin contents have been chosen for comparison. The types of weaves selected are plain weave, satin weave, and tridirectional weave. The composites made of the fabrics have been compared to composites made from unidirectional tapes under static and fatigue loading. During static loading acoustic emission events have been monitored. Also, examinations of fracture surfaces and polished sections both away from the fracture surface, and of virgin specimens under an electron microscope have been discussed.

TABLE OF CONTENTS

INTRODUCTION

The future high cost and limited availability of energy has resulted in the need for designing aircraft that can maintain the present levels of performance with a decrease in the level of fuel consumption. One way of fulfilling this need is by using materials that offer a higher strength - to - weight ratio than are offered by the currently used aircraft structural materials. Advanced graphite-epoxy composites offer such a potential. Preliminary projections indicate[1] that as much as a twenty percent reduction in weight is possible in the design of airframe subassemblies by using graphite-epoxy composites. Such a reduction of weight in the airframe subassemblies can lead to a reduction of gross take-off weight in the range of five to fifteen percent. Similarly a development of advanced composites that are capable of operating at high temperatures might improve the thrust-to-weight ratio by as much as twenty-five percent[2]. Such an improvement leads to an additional reduction of gross take-off weight by an amount larger than ten percent[2].

These potential benefits have resulted in an increased research activity among structures and materials engineers. Some of the research activities are connected with the environmental effects, the techniques of decreasing the cost of production, the development of nondestructive inspection procedures, the techniques of life estimation, the development of fail-safe design procedures, foreign object damage, the damage tolerance, and the dynamic properties of composites.Most of the investigations in the field of graphite-epoxy composites have been conducted with unidirectionally reinforced lamina or laminates. However, graphite-epoxy composites can be produced by using single or multiple layers of woven graphite fabrics and epoxy. Very little work has been

reported in the field. Most of the reported work is concerned with the fabric and not composites.[2-8]. These woven graphite-epoxy composites offer a potential reduction in the cost of production of actual structures.[9] For example, the use of woven fabric concept in fabricating NASA telescope metering truss has resulted in a reduction in the cost of labor from two-man days to two hours. Other potential benefits of woven graphite-epoxy composites include a lower probability of delamination than in uniaxial reinforced composites. Inspite of these potential benefits there is very little research work reported in this field. Therefore, an investigation leading to the comparative evaluation of the woven graphite epoxy composites is being conducted by the authors. This paper describes the results of the investigations.

PROBLEM SETTING

Woven fabric composites or woven composites consist primarily of woven fabrics and epoxy. Different woven fabric composites are characterized by the different type of weaves, different percentages of epoxy in the composite, different stacking sequence, different number of layers and different geometry. In this report, the evaluation of woven composites is restricted to different types of weaves and different percentage of resin content. In particular, plain weave, (Figure 1a) satin weave (Figure 1b) and tri-directional weave (Figure 2) have been considered whenever possible. The mechanical properties of these composites have been compared to those made from unidirectional tapes. Different resin contents varying from 20 to 50% have been considered for purposes of evaluation of woven composites. Only tensile loading and fatigue loading have been considered. The mechanical properties to be evaluated and compared include the failure stress, the specific failure

strength, and the acoustic emission behavior. In addition to the investigation of these mechanical properties, the study also includes the analysis of the facture surfaces by using a scanning electron microscope. The acoustic emission has not been considered for the case of fatigue loading.

SPECIMEN PREPARATION

Weaving

The first task of the project was to develop a capability to weave graphite fabrics from graphite yarns at Georgia Tech. In particular, the capabilities for producing fabrics of plain weave, satin weave and tri-directional weave were sought. The plain weave fabrics and the satin weave fabrics were produced by using hand loom techniques at Georgia Tech. The choice of hand loom was because of the non-availability of a proper power loom that would assure prevention of damage to graphite yarn. Union Carbide's Thornel 300 that has 3000 fibers per yarn was used. The production started by winding the yarn off the commercial spool on to a single ended warper. This operation was done to produce evenly spaced yarns that were eventually wound on a warp beam for purposes of weaving. In the whole process, the major emphasis was on the protection of graphite fibers. A layer of paper was wound between the layers of graphite yarn to prevent the rubbing of yarns. Several glass rod guides were used to control the movement of warp yarn. All fabric had equal number of yarns in warp and fill directions. The looms were capable of producing fabrics of different ends per inch. The single end warper was also used to produce unidirectional tapes of desired number of ends per inch.

In order to compare with the plain and the satin weaves of twelve or more end per inch, a fabric of tri-directional weave of comparable

ends per inch was needed. In order to achieve this objective, the School of Textile Engineering at Georgia Institute of Technology bought a Gloor Triweave machine. However, the investigators had difficulties in adapting the machine for producing graphite fabrics of tridirectional weave. The principal reasons for the difficulty in adapting the machine for graphite yarns were the complicated yarn path and coarse eyelets. These difficulties were eliminated by designing a set of copper tubes for guiding yarn. It was also demonstrated that the use of copper tubes would eliminate the possibility of damage to graphite yarn. However, 188 such tubes needed to be installed for obtaining the desired ends per inch. It was not possible to install the desired number of tubes during the project. As an alternative, tridirectional frame weaving technique was used to produce the needed fabrics for the project. The details of the frame weaving technique are illustrated in figures 4, 5, and 6. Figures 4 and 6 illustrate the warp yarns at $+30^{\circ}$ and -30° and fill yarns at 90°. The only difficulty with frame weaving was that the finished fabric was restricted to 7 ends per inch. This restriction is imposed because of the maximum area of the overlapping triangle (See figures 2 and 4). The figure 5 depicts the size of the warp yarn sheets necessary to produce a net size of 12" x 12" fabric.

Fabrication

The process of production of both the plain and satin weave panels was very nearly the same with minor exceptions. First, the fabric was cut into properly sized sheets, 9½" x 12", with the 0° axis being in the warp direction. The sheets were then weighed individually to obtain the total fiber weight, and to determine the amount of resin needed. The solid epoxy resin was combined with acetone, which was used as the solvent, in a 50/50 mixture and stirred for a minimum of three hours as recommended by the manufacturer. Acetone was added periodically to maintain the correct ratio. The sheets

of fabric were then impregnated with the resin solution by pouring the solution (amount equalling twice the weight of the fabric) over the fabric and then rolling with an aluminum roller to ensure penetration into the weave and fibers. The sheets were then set aside to allow the acetone to evaporate for twelve hours or more. At the end of this period, the sheets would ideally be a 50/50 ratio of fiber to resin with allowance of 2% for roll-off and the excess acetone which did not evaporate.

The stacking sequence is shown in Figure 7 and will be briefly explained for each laminate. The area of the base plate containing the laminate was enclosed by a cork dam, and the surface within the dam was coated with a release agent. A layer of 1 mil. teflon was next put on the plate to eliminate bonding of laminate to plate. The graphite/epoxy fabric sheets were laid up outside the dam and then placed within after rolling with rubber roller to remove trapped air. The stacking sequence was the same for woven panels with the warp direction being the 0^{o} axis or longer dimension. The laminate was sandwiched between layers of TX1040, a pourous teflon-coated release cloth again to prevent cobonding of laminate to plate or bleeder material. The bleeder material was placed directly above the TX1040. The required amount of bleeder material was calculated by weighing the laminate immediately prior to debulking, thereby determining the excess resin actually contained. The bleeder sheets, 181 and 120 glass, were then selected in the proper ratio to absorb this resin.

Topping the bleeder material was another layer of teflon on to which was placed the perforated, release-agent coated top aluminum plate. This lay-up assembly was sealed by placing a commercial sealer strip between top plate and cork dam. Through the holes in the top plate,holes were

punched in the teflon layer below to allow for excess bleeding. The entire assembly was then placed in a vacuum bag composed of two sheets of 2 mil mylar and a sealer before connecting to a pump for 2 hours.

A slightly different stacking sequence was designed for tri-directionally woven composities. Such a sequence was designed by taking into account the limited quantity of available tri-directional fabric. These composites were made from four layers of tri-directional fabric and three layers of satin fabric. The layers of satin fabric were used as the outer and the central layer.

For purposes of comparison, composites were made from unidirectional tapes. For example, to compare a woven composite consisting of 8 layers of plain weave fabric, a composite consisting of 16 layers of unidirectional tape and an appropriate stacking sequence was produced. Similarly tapes were laid at $+30^{o}$, -30^{o} and 90^{o} to produce composites for comparing with tri-directionally woven composites.

Different resin contents were obtained by controlling the initial amount of epoxy used, temperature of a drying cycle that was used prior to curing, the pressure and temperature of the final curing cycle.

Curing

This phase consisted of stacking the lamina in prescribed sequence and then placing the laminate in an oven for about 2 hours at 373^{o} K to evaporate the acetone. The prepreg staging has a great influence in controlling the quality of the laminate. The cure cycle is as follows:

1. Pre-cure for 2 hours at 373^{o} K, allow to cool
2. Vacuum bag entire assembly

3. Apply full vacuum for 2 hours to debulk at room temperature
4. Maintain vacuum throughout entire cycle
5. Place in press and raise temperature to 394° K at 1°-3° K per minute under minimal pressure
6. Hold at 394° K (3°-6° K) for 15 ±5 minutes, apply 690 kPa (34-0 kPa)
7. Hold at 394° K (3°-6° K) and 690 kPa (34-0 kPa) for 45 ±5 minutes
8. Increase the temperature to 450° K (6°-0° K) at 1°-3° K per minute
9. Hold at 450° K (6°-0° K) for two hours ±15 minutes
10. Cool under pressure and vacuum to below 353° K

For individual laminates the step (1) and the pressure in the final curing cycle varied.

Tensile Specimens

The panels were first trimmed 25 mm on all sides to prevent non-uniformities in thickness. The panels were then cut into specimens by use of an abrasive wheel. The final dimensions were obtained by grinding with a diamond wheel. Examination of the edges of all specimens showed no rough surfaces or notches. The dimensions of each specimen, in accordance with ASTM specifications: length = 254 mm, width = 25.55 mm, was maintained whenever possible.

Aluminum tabs measuring 38.1 mm in length by 3.18 mm thickness and 25.4 mm wide with a 15° bevel were bonded to the specimens with Eastman 910 adhesive.

TESTS

All tensile tests under static loading were conducted in an Instron Universal Testing Machine. The speed of the cross head was set to provide a strain rate within the tolerances of A.S.T.M. specifications. Several laminates were instrumented with strain gages for monitoring

the stress-strain behavior. During most of the tests acoustic emission was monitored by using Dunegan/Endevco 3000 series equipment. Two transducers were mounted near the tabs of the specimen to serve as guard transducers for purposes of filtering the signals that have sources outside the gage length of interest. A central transducer was mounted to monitor the acoustic emission data. With the exception of tests numbered 42-52, the guard transducers were Dunegan/Endevco S 140 B/HS and the data transducer was Dunegan/Endevco S 140 B. Because of the reduced gage lengths in the tests 42 to 52, Acoustic Emission Technology micro-miniature transducers MC 500 were used as guard transducers and DE S140B/HS was used as data transducer.

A data acceptance region was established by both guard transducers and the data transducer. Events that occurred outside the region did strike the guard first. As a consequence, the data collection process was shut down and the unwanted signals such as the grip noise were eliminated. On the other hand, an event originating within the region of acceptance created a pulse that did strike the data transducer first and produced a signal which passed through a 40 db preamplifier, a band pass filter, an adjustable gain amplifier, a threshold counter and a distribution analyzer. Accepted cumulative events and counts were plotted on an x-y plotter.

The tensile fatigue tests were conducted in an M.T.S. system. The specimens, used for fatigue tests, had a central hole of 6.35 mm diameter. The specimens from the same batch with an identical central circular hole had been tested in an Instron Testing Machine to obtain static ultimate strength. The specimens were tested at a mean load of 85% of this ultimate strength. An oscillating load of $\pm$ 10% of the ultimate load was selected.

All specimens were tested at 30 cycles per second.

After completion of the testing program, the fracture surface of one specimen of each type of laminate was examined by using a scanning electron microscope ISI-60. The fracture surfaces were mounted on aluminum stubs and coated with gold before examination. Similar examinations were conducted on (a) sections from fractured laminates taken away from the fracture surface and (b) sections from unfractured laminates for purposes of comparison. These sections were first mounted in epoxy and then polished. The polished specimens were later coated with gold for S.E.M. examination. The useful magnifications varied from 50X to 30,000X. Selected areas were photographed.

RESULTS AND DISCUSSION

Static Tests

The Table I shows the results of all recorded tests. The test numbers are not in sequence. This is necessary to group the type of weave and resin content. The table displays the percentage of resin content by weight, the type of weave, lay-up, thickness, gage length, ultimate load, the total detected acoustic emission events, and the total detected acoustic emission counts over a fixed threshold of one volt after the selected amplification and filtering operations. A double asterick is used to indicate specimens with holes.

The Table II illustrates the group mean values of ultimate stress in Newtons/meter^2 or N/m^2 and the standard deviation. Similarly Table III illustrates the group mean values and standard deviation for ultimate stresses for specimens with circular holes. The values of standard deviation from Table II indicate an appreciably lower scatter in woven composites when compared with the unidirectional composites. When plain weave and satin weave are compared, the satin weave specimens offer a lower scatter.

The tri-directional weave has the lowest scatter in the observed results for woven samples. As expected, the ultimate stresses for plain woven composites are lower than that of unidirectional composites. In some cases, the satin weave with more ends per inch but same total weight of fiber, has the highest ultimate stress of tested specimens. This weave offers the advantages of fabrication that are characteristic of woven composites while retaining the strength. The reduction in strength of plain weave almost disappeared when a stress concentration in the form of hole is present. However, in the conducted tests, satin weave displayed a lower strength in the presence of a hole when compared with unidirectional specimen of the same resin content. However, the number of samples tested was small to draw any specific conclusions.

The Table IV illustrates a comparison of specific strengths with the type of weave and the resin content. The specific strength is defined as the ratio of strength in N/m^2 to the density in grams per cubic centimeter. The table is arranged in decreasing order of specific strength. All results in this table are for specimens without stress concentration. Under tensile loading, 30.2% satin weave offers the best specific strength or strength to weight ratio of the tested specimens. These specimens, however, had higher ends per inch. The 30% plain weave has only a reduction of 6% specific strength when compared to unidirectional weave. The two ultimate strengths are much closer to one another when holes are present. The tri-directional weave displays the lowest strength of all weaves with resin content in the range of 30-37%. The low values are due to the low end per inch, very open weave providing areas for large matrix concentration thus weakening the laminate. Tables V and VI illustrate the comparison of modified ultimate stress. This comparison was done in addition to the specific strength for the following reasons.

In calculating specific strength, the value of density was needed. These densities were calculated for a given panel. However, the thicknesses were measured accurately for each specimen. Then the two ultimate strengths can be compared by assigning a weight based on the density ratio. The modified ultimate stress is then derived as follows:

$$\sigma_{mu} = \frac{\sigma_u \, t_G}{t_{G\,min}}$$

In the equation, t_G is average group thickness and t_{Gmin} is the lower of two t_G values. It is to be noted that the width of each specimen was the same. The total number of yarns in each panel was the same. Then for the same total number of yarns same width and length, the thickness of the woven composite is usually more. The resin content being the same, the thickness controls the strength to weight ratio. On this basis, the reduction in specific strength is of the order of 3-6% for specimens without holes. For specimens with holes, woven specimens have higher strength. However, it is to be noted that the number of tests with holes was small.

Acoustic Emission

The figure 8 illustrates the plot of acoustic emission events versus time for composites containing 37% resin content and made of plain weave fabric. The cross head speed for these tests was .25 cm minute. The results of tests 15, 16 and 17 displayed almost identical results during the first half of the test duration. The number of events differed only by about 10% during the next fifteen seconds for these tests. Later, the plots separate as failure approaches. These specimens with nearly identical plots also had failure loads within 5% of each other. The failure loads were 25354, 25577 and 24465 Newtons. The specimen 10, however, displayed increased early emission activity. The emission rate

increased faster than that for the group 15, 16, and 17. The increase of acoustic emission activity suggests the possibility of preexisting damage or a substandard specimen. This hypothesis is supported by the lowest failure load of 18682 N. for this group. The specimens 15, 16 and 17 had an average failure load of 25132 Newtons. The acoustic emission event pattern for specimen 3 shows an increased early emission activity somewhere between the "standard pattern" of the specimens 15, 16 and 17 and an extreme pattern of the specimen 10. However, for a short time, the pattern appears to return to the standard pattern only to display an increased emission rate during the middle of the test. The increased early emission activity and an increased emission rate during the middle of test suggest the possibility of damage or substandard specimen. The quality of the specimen can be expected to lie between the standard and the extreme of the specimen 10. This hypothesis is again confirmed by the failure load of 22686 Newtons which is between the average of 25132 Newtons and the lowest value 18682 Newtons for the specimen 10.

The figure 9 illustrates the plot of acoustic emission events versus time for a composite made of plain weave containing 22% resin. This is the only specimen of this type for which the acoustic emission has been monitored. The results will be compared with the specimens of plain weave and 37% resin. This plot follows the pattern of the test number 10 rather than the "standard" of figure 8. The ultimate load again is 18015 Newtons which is quite close to that of specimen 10 which is 18682 Newtons. The resin content of 22% rather than 37% can be considered as the substandard quality of the specimen. Thus, these two figures indicate that the early emission activity compared to a standard and the increased activity during the middle of the test is an indication of the quality of the specimen.

The figure 10 shows the plot of acoustic emission events versus time for three composites containing 50% resin and plain weave fabric. The cross head speed is again .25 cm per minute. The specimens 12 and 13 initially follow the "standard emission pattern" of specimens 15, 16, and 17 as illustrated in figure 8. However, the emission rate increases during the middle of the test. The increased rate lies some where between that of the standard pattern and the extreme of test number 10. The failure load for these specimens has a mean of 20684 Newtons. This value is higher than the extreme case of the test 10 and lower than the considered standard of tests 15, 16, and 17. The acoustic emission pattern of the test 4 is different. It shows an increased emission rate during the middle of the test. This activity decreases later. The specimen had an ultimate load of 22241 Newtons. The sudden switch in the emission rate also coincides with higher ultimate load. Both the failure load and the event plot for this test are very similar to test 3. The key points useful in comparison appears to be the departure from the "standard" acoustic emission events and the standard emission rate.

The figure 11 shows the variation of acoustic emission events versus time for tri-directional weave. It is to be noted that the fabric used in this case had only seven ends per inch. Because of the open weave large spaces for matrix concentration and voids are available. The tests were conducted at a cross head speed of 0.13 cm per minute. The resulting acoustic emission plots are well grouped. All specimens are of the same quality. The specimen 50 which has the highest rate of emission activity during the early part of the test had the lowest failure load in the group. The specimen 49 which had the lowest emission rate during the early part of the test had the highest failure load in the group. As

a group, the emission activity can be be compared to the plain weave composites containing 37% resin content (figure 8). After appropriate corrections for the cross head speed the average emission rate for tridirectional specimens is approximately twice that observed for the "standard pattern" of the specimen 15, 16, and 17 of figure 8. It is also to be noted that the average failure load for the tridirectional specimens is 13122 Newtons and the average failure loads for specimens 15, 16, and 17 is 25132 Newtons.

The figure 12 shows the acoustic emission events variation for composite specimen prepared from unidirectional graphite tapes and containing 37% resin. These plots display considerable scatter just like the scatter in the failure loads displayed in the Table I. The cross head speed for these tests was .25 cm per minute. The figure 13 shows the acoustic emission results for a composite made from unidirectional tape and containing 50% resin. The results of this series of tests are best analyzed by beginning at the fabrication stage. As mentioned earlier, this panel was precured before the final cure cycle began. A higher precuring temperature than normal was responsible for high resin content. Therefore, many air bubbles were trapped causing visible voids. This high void content greatly reduced the strength of the specimens. The acoustic emission event graphs of figure 13 show that specimen 14 has early activity over a short period followed by gradual increase in slope, while specimens 5 and 18 do not show activity until much later time. The patterns of specimens 5 and 18 can be seen to be nearly identical with the exception of the sharply increased activity of specimen 18 before failure which is not uncommon. Discounting the initial spurt of events in test 14, this path coincides closely with the other two with exception that the rate of increase of the slope is higher as failure approaches. All specimens

show a marked increase in event rate shortly before failure. The failure loads reflect the emission rates; the loads are not identical but grouped reasonably well. The fact that there are fewer acoustic emission events in a poor quality specimen is suprising.

The figure 14 shows the acoustic emission events for specimens with holes. The tests 21 and 22 are for composites of plain weave with 37% resin and 6.35 mm diameter hole. The specimen 23 is a composite from plain weave fabric and 50% resin. The specimen 24 is a composite prepared from unidirectional tapes and 37% resin with a hole of 6.35 mm diameter. The number of tests of this particular type are too few to provide any comparison.

Fractography

Fracture surfaces of various laminates were examined under the scanning electron microscope, model ISI-60. This examination is not intended to qualify the specimens but to study the surfaces and determine if any additional information can be obtained from this method of inspection. Several interesting features were observed; some pertaining to possible explanation of failure and others on fiber surface pattern differences. Figures 15, 16, 17 and 18 are the magnified pictures of fracture surface of a composite from plain weave fabric and containing 22% resin. Similar observations have been made on fracture surfaces of plain weave fabric containing 37% resin. This particular specimen has a failure load of 18015 Newtons much less than the average load for good quality specimen which is 25132 Newtons. The S.E.M. examination is conducted to explain the reasons for the low failure load.

The figures 15 and 16 show the voids. In particular, the figure 16 shows the oval shaped smoothly contoured areas. The figure 15 shows areas where there were pre-existing fiber breaks before the composite

was produced. The figure 17 shows the origin of delamination. The figure 18 is the magnified image of a portion of the fracture surface at 12K. A single fiber can be observed. This figure shows the normal tension failure of a single fiber. A smooth area at the crack origin followed by radial lines, can be observed. It is to be noted that there is a small hole at the crack origin. This is hypothesized to be a pre-existing flaw in the fiber where the tension failure originated.

The figure 19, 20 and 21 are for a composite of 50% resin and plain weave. Figure 19 shows a type of propagation of cracks through the fiber bundle. The crack origin is at the junction of two fibers. A change in the direction of propagation at the upper left fiber and the right fiber can be seen. However, at the junction of the lower left fiber and the right fiber, the crack propagates without change of direction.

The figure 20 shows the damage to a complete bundle of fibers incurred before curing. Near the upper edge,many little bumps are seen. These are actually bundles of broken fibers which have been coated with a matrix in the curing process. The decrease in strength locally would be severe. The figure 21 shows several partially damaged bundles. The damaged regions do not appear clean and sharp, instead the fibers look as they have been mashed down. Also, the delamination arrested by the weave pattern in upper left corner around the 0^{o} fiber and following the transverse fiber can be seen in this figure.

The figures 22 and 23 are from a plain weave specimen which showed very poor failure load. The reason for this can be observed in the pictures. The specimen shows extreme fabrication damage. In figure 22 and 23 well over half of the available 0^{o} bundles were broken and covered with matrix. These are the bumps on the surface. The figure 24 shows how the cross-section should normally look. The figure 24a is for 37%

plain weave shown for comparison. The fracture surface is smooth no large pull-outs. This specimen of figure 24a had one of the very high failure loads.

The figure 25 is a magnified picture of a polished section of a composite specimen of plain weave fabric and 37% resin. The section is 38 millimeters away from the fracture surface. No unusual fracture pattern is observed. In fact figure 25 is very similar to figure 26 which is the magnified picture of polished section of an unfractured or virgin specimen. The figures 25 and 26 are at approximately 5K magnification. The figure 27 is a lower magnification picture of a section from a virgin specimen. The fiber bundles, as they appear in woven composites, can be seen. The figure 28, however, is from a section of failed composite 5MM from the fracture surface. This picture is from a polished section at a magnification of 9.8K. Some cracks at the fibermatrix interface can be seen. A large number of fibermatrix interfacial cracks can be seen at 1K as shown in the figure 29. This figure can be compared to the figure 30 which shows no such cracks. The figure 30 is, however, from a section of a virgin specimen. In the next few figures, the plain weave fracture surfaces have been compared to the fracture surfaces from composites made from unidirectional tapes. The figure 32 shows the view of a cross section with double 0^{o} layer at the center and 90^{o} ply on the outside. This picture can be compared to the figures 16 and 17 of plain weave. The clean appearance of 90^{o} plies can be seen. Also no arrest of any delamination can be seen. The figures 31 and 33 show fractured single fibers. Pre-existing flaws can again be seen at the crack origin in both pictures.

The figures 34 to 36 show the magnified pictures of fracture surface from composites made from tri-directional weave fabrics. The resin content

of these specimens is 31.7%. Figures 34 and 35 are high magnification pictures of single fiber fracture surfaces. The fiber shown in Figure 34 exhibits a nearly smooth surface, lacking the surface irregularities common to tensile failure patterns. Similarly figure 35 displays an unusual fracture pattern. The figure 36, however, shows typical tension failure of fibers observed in other types of composites.

Fatigue Failure

Only five specimens were tested in tension fatigue. The specimens are mainly used to study the fracture patterns under a scanning electron microscope. All fatigue specimens are from composites from plain or satin weave fabrics. The resin content varied from 31 to 34 percent by weight. All the specimens had a central hole.

The inspection under S.E.M. is restricted to the area near the fatigue crack origin which was near the hole. The figures 37 to 44 show the fracture pattern of single fibers under magnifications varying from 2.0K to 15K. The fracture patterns of these fibers are very distinct from the fracture patterns of the fiber under static tensile loading as can be seen in figures 18 and 19. The fracture patterns of these fibers are characterized by a smooth area over substantial part of the fiber. Also no stress concentration such as a hole is seen at the crack origin. They appear to be cracks originated by fatigue. However, more tests are needed to confirm the hypothesis. Away from the crack origin standard tensile fracture patterns were observed. The figure 40 shows a number of such unusual fracture patterns. Similar observations on plain weave composites can be seen in figures 41 to 44.

CONCLUSIONS AND RECOMMENDATIONS

The woven fabric composites display specific strengths only slightly below that of composites made from unidirectional tapes. This fact

combined with a low scatter in the results and a potential for saving labor cost in fabrication makes the woven composites quite an attractive candidate material for aircraft structures. The satin weave combines the advantages offered by the woven composites and high strengths of unidirectional composites. However, plain weave specimens have practically no delamination displayed on the fracture surface. The tri-directional weave, even though containing only 7 ends per inch, displayed comparable strength. A closer weave can make this a very attractive candidate material. Nondestructive inspection procedures for quality control, estimation of ultimate load, comparative evaluation of composites, and flaw detection procedures can be established by using acoustic emission and emission rates. However, additional investigation, including quantitative models, are necessary.

A preliminary observation indicates that woven composites may be superior to unidirectional composites in fatigue behavior. Further work is necessary. Observation under scanning electron microscope provides tools for failure analysis and quality control. In addition, it may prove possible to distinguish fatigue failure from other failure modes by use of fractographs. The quality control can be done by testing fractured and unfractured sample specimens from each batch of production.

REFERENCES

1. _____, "Work Shop on the Effects of Relative Humidity and Elevated Temperature on Composites," Sponsored by AFOSR, Newark, Delaware, March, 1976.

2. Ko, W. L., "Fracture Behavior of a Nonlinear Woven Fabric Material," J. of Composite Materials, Vol. 9, p. 361, 1975.

3. J. Skelton, "Strength of Textile Structures at High Strain Rates," J. Materials, Vol. 6 (1971), p. 634.

4. D. Roylance, "Ballistic Impact of Textile Structures," Text. Res. J., Vol. 43 (1972), p. 34.

5. W. C. Sleeman and T. G. Gainer, "Status of Research on Parawing Lifting Decelerators," J. Aircraft, Vol. 6 (1969), p. 405.

6. N. J. Abbott and J. Skelton, "Crack Propagation in Woven Fabrics," J. Coated Fibrous Materials, Vol. 1 (1972), p. 234.

7. W. D. Freeston and W. D. Claus, "Crack Propagation in Woven Fabrics," J. App. Phys., Vol. 44 (1973), p. 3130.

8. A. D. Topping, "The Critical Slit Length of Pressurized Coated Fabric Cylinders", J. Coated Fabrics, Vol. 3 (1973), p. 96.

9. _____, "Aviation Week, McGraw-Hill, New York, Jan. 26, 1976.

TABLE I

Test	Resin Content (%)	Material Layup	Thickness (mm)	Total Counts	Total Events	Gage Length(mm)	Ult. Load(N)
3	37	PW (12x12) 8ply	1.60	511276	13843	177.8	22685.9
7	37	PW (12x12) 8ply	1.65	NA	NA	177.8	21796.3
10*	37	PW (12x12) 8ply	1.55	191290	17320	177.8	18682.5
15	37	PW (12x12) 8ply	1.73	916076	30466	177.8	25354.8
16	37	PW (12x12) 8ply	1.50	500,000	18,651	177.8	25577.3
17	34.4	PW (12x12) 8ply	1.52	565676	25738	177.8	24465.2
21**	37	PW (12x12) 8ply	1.70	13218	1461	177.8	11787.8
22**	35	PW (12x12) 8ply	1.56	31986	3025	177.8	11343.0
6	37	UD^{+}(90.0.90.0.90.0.90.0)s	1.52	178391	44415	177.8	29803.1
9*	37	UD^{+}(90.0.90.0.90.0.90.0)s	1.45	264929	20447	177.8	23575.6
11*	37	UD^{+}(90.0.90.0.90.0.90.0)s	1.46	104179	4978	177.8	17792.9
24**	37	UD^{+}(90.0.90.0.90.0.90.0)s	1.42	19909	1551	177.8	10230.9
25	37	UD^{+}(90.0.90.0.90.0.90.0)s	1.45	41126	2679	177.8	20328.4
4	50	PW (12x12) 8ply	2.22	158556	10231	177.8	22241.1
2*	50	PW (12x12) 8ply	2.16	376391	14743	177.8	21129.1
13*	50	PW (12x12) 8ply	2.16	259081	14499	177.8	20239.4
23**	50	PW (12x12) 8ply	2.16	10567	1099	177.8	10453.3
5	50	UD^{+}(90.0.90.0.90.0.90.0)s	2.23	43249	1540	177.8	17348.1
14	50	UD^{+}(90.0.90.0.90.0.90.0)s	2.26	66100	2003	177.8	15568.8
18	50	UD^{+}(90.0.90.0.90.0.90.0)s	2.29	20755	649	177.8	14990.5
27**	50	UD^{+}(90.0.90.0.90.0.90.0)s	2.34	NA	NA	177.8	9674.9
28	31	Satin (12½x12½) 8ply	1.52	060	NA	177.8	22241.1
30**	31	Satin (12½x12½) 8ply	1.52	NA	NA	177.8	11476.4
1	18	PW (12x12) 8ply	1.35	3174	159	177.8	15123.9
2	18	PW (12x12) 8ply	1.30	66720	1992	177.8	16903.2
8	22	PW (12x12) 8ply	1.40	1000000	33613	177.8	18015.3
20**	22	PW (12x12) 8ply	1.32	91989	5799	177.8	8896.4
26**	30	UD^{+}(90.0.90.0.90.0.90.0)s	1.22	NA	NA	177.8	8785.2

32*	30.4	PW (12x12) 8ply	1.47	280100	Not Recorded	177.8	21017.8
33*	30.4	PW (12x12) 8ply	1.49	305659	Not Recorded	177.8	23353.2
34	30.4	PW (12x12) 8ply	1.50	428474	Not Recorded	177.8	24465.2
35	30.4	PW (12x12) 8ply	1.50	369229	Not Recorded	177.8	24020.4
36	30.4	PW (12x12) 8ply	1.50	228196	Not Recorded	177.8	19794.6
37*	30.2	Satin (24x23) 4ply	1.40	117441	Not Recorded	177.8	24687.6
38*	30.2	Satin (24x23) 4ply	1.42	119799	Not Recorded	177.8	21796.3
39	30.2	Satin (24x23) 4ply	1.36	126746	Not Recorded	177.8	24910.0
40	30.2	Satin (24x23) 4ply	1.40	101842	Not Recorded	177.8	23130.8
41	30.2	Satin (24x23) 4ply	1.30	132907	Not Recorded	177.8	22685.9
42	30.3	5.-30.90.30.5.30.90.-30.5	1.47	556525	21308	101.6	24020.4
47	30.3	5.-30.90.30.5.30.90.-30.5	1.46	152707	6615	101.6	18793.7
44	30.3	5.-30.90.30.5.30.90.-30.5	1.50	510549	22426	101.6	23041.9
45	30.3	5.-30.90.30.5.30.90.-30.5	1.45	567361	21790	101.6	23041.9
46	30.3	5.-30.90.30.5.30.90.-30.5	1.47	191975	11895	101.6	21262.5
43**	30.3	5.-30.90.30.5.30.90.-30.5	1.42	46988	2392	101.6	10809.2
48**	30.3	5.-30.90.30.5.30.90.-30.5	1.47	39543	1504	101.6	10230.1
49	31.7	Tri-Directional[1]	1.63	814386	23753	104.78	14234.3
50	31.7	Tri-Directional[1]	1.63	327140	8396	104.78	11565.4
51	31.7	Tri-Directional[1]	1.60	414849	11748	104.78	12143.6
52	31.7	Tri-Directional[1]	1.60	805528	21783	104.78	14189.8
29	31.7	Tri-Directional[1]	1.60	NA	NA	104.78	13567.1
31**	31.7	Tri-Directional[1]	1.60	NA	NA	104.78	8896.4

* - Strain Data Available

** - 6.35mm Diameter Hole @ Center

\+ - 12 Ends/Inch

PW - Plain Weave Fabric

UD - Unidirectional Prepreg Tape
12 Ends/Inch

Note 1: The tridirectional specimens layering configuration is satin/$3D_2$/satin/$3D_2$/satin where the 3D layers are woven graphite yarn with 7 ends/inch oriented -30/90/30 degrees to the tensile axis. The 30.3% resin specimens were produced to compare with this laminate also using 24x23 satin weave; designated "satin" Table I tests 42-48.

TABLE II

Group Values For Specimens Without Holes

Resin Content (%)	Material Configuration	Ultimate Stress (N/m^2)	Standard Deviation	(N/m^2) for Fiber in Loading Direction
37	Plain Weave	572416532	72119160	1144833065
37	Unidirectional	654595143	109185375	1309190287
50	Plain Weave	382783130	12644984	765566260
50	Unidirectional	278286190	24490177	556572380
18	Plain Weave	478013516	50497201	956027033
22	Plain Weave	507702341	0	1015404682
30.4	Plain Weave	594845177	52131259	1189690355
30.2	Satin Weave	672411195	45994925	1344822392
30.3	Satin/Unidirectional	589729267	54075580	1173529044
31.7	Tri-directional	321302580	30343826	399351231
31	Satin Weave	574560801	0	1149121603

TABLE III

Group Values For Specimens With Holes

37	Plain Weave	279285929	9314816	558571859
37	Unidirectional	283174573	0	566349145
50	Plain Weave	190619352	0	381238704
50	Unidirectional	162998955	0	325997909
22	Plain Weave	265179256	0	530358513
30.3	Satin/Unidirectional	286297898	18215948	560343812
31.7	Tri-directional	218880962	0	269192005
31	Satin Weave	213737473	0	427474946
30	Unidirectional	283684785	0	567369570

TABLE IV

Comparison of Specific Strengths

Specimen Type	Specific Strength (10^4m)
30.2% Satin Weave (24 x 23)	4.4821
37% Unidirectional Tape	4.3208
31% Satin Weave (12 x 12)	4.0574
30.4% Plain Weave	4.0325
22% Plain Weave	4.0183
30.3% Tridirectional Simulation	3.9113
37% Plain Weave	3.7562
18% Plain Weave	3.5832
50% Plain Weave	2.7140
31.7% Tridirectional Weave	2.2939
50% Unidirectional Tape	1.9665

TABLE V

Comparison of Group Modified Ultimate Stress

Specimens Without Holes

Specimen Type	Modified* Ultimate Stress (N/m^2)
37% Plain Weave	620941833
37% Unidirectional Tape	654595143
50% Plain Weave	382783130
50% Unidirectional Tape	288662799

Specimen Type	Modified+ Ultimate Stress (N/m^2)
30.4% Plain Weave	616405083
30.2% Satin Weave	672411195
31.7% Tridirectional Weave	351818775
30.3% Tridirectional Simulation	589729267

TABLE VI

Comparison of Group Modified Ultimate Stress

Specimens With Holes

Specimen Type	Modified* Ultimate Stress (N/m^2)
37% Plain Weave	320426946
37% Unidirectional Tape	283174573
50% Plain Weave	190619352
50% Unidirectional Tape	176416152
31.7% Tridirectional Weave	241916345
30.3% Tridirectional Simulation	286297898

* Modified Ultimate Stress defined to be: $\frac{t_G\,(\sigma_u)}{t_{min}}$

t_G = group average thickness

t_{min} = lower of two t_G values

+ Modified Ultimate Stress defined to be: $\frac{\rho_G\,(\sigma_u)}{\rho_s}$

$_G$ = density of either group

$_s$ = density of satin and simulation groups respectively

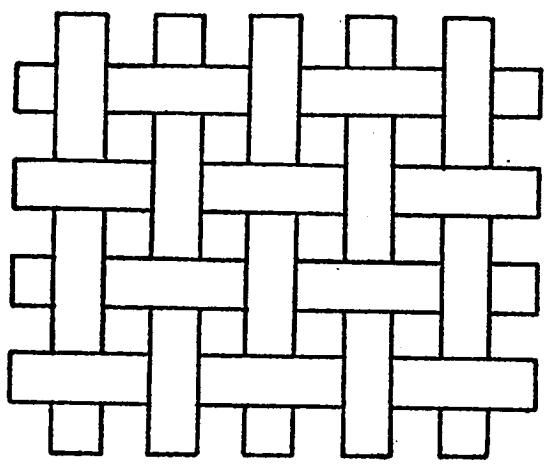

Fig. la Plain weave fabric

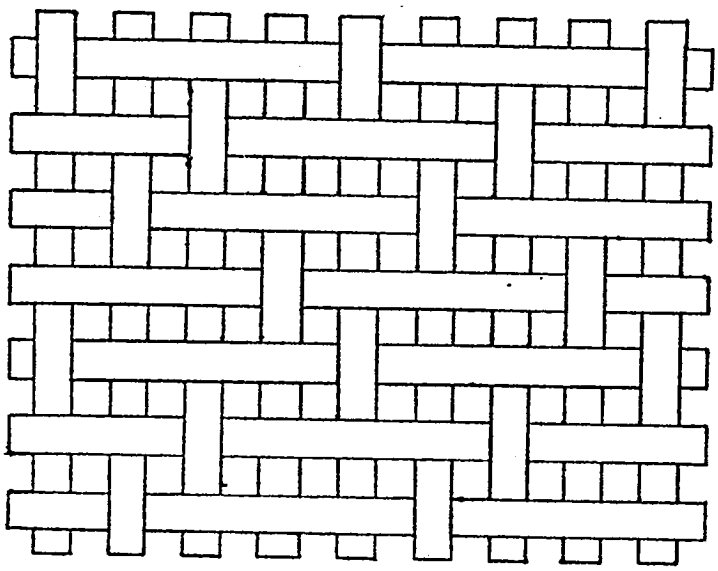

Fig. 1b Satin weave fabric

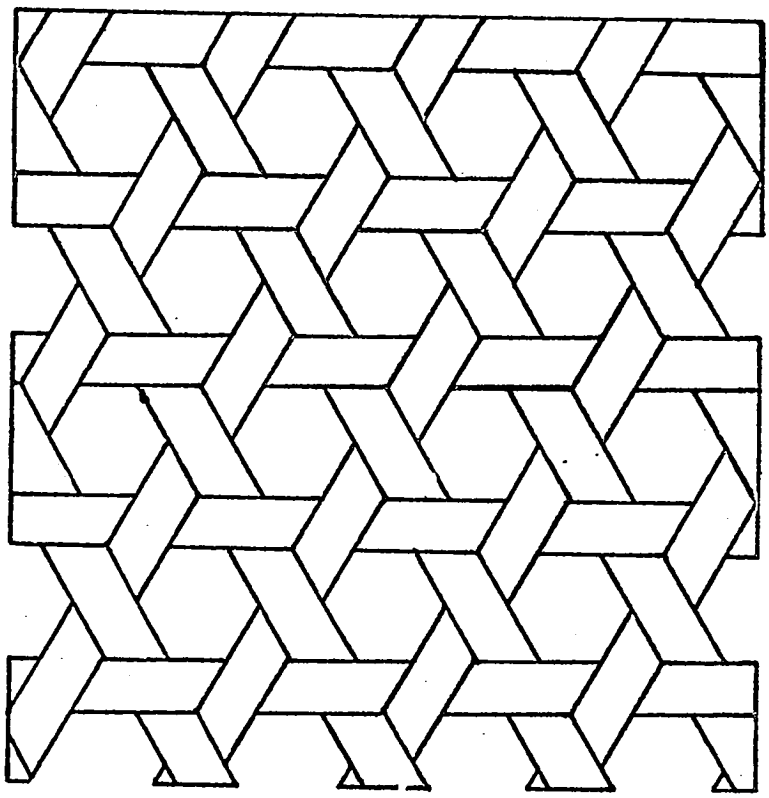

Fig. 2 Tri-directional fabric

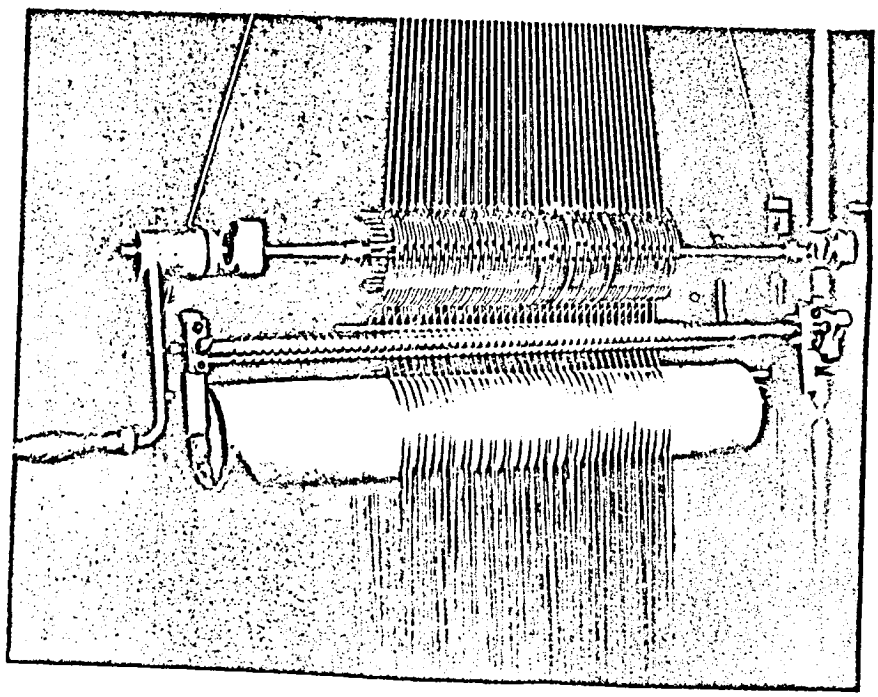

Fig. 3 Hand loom

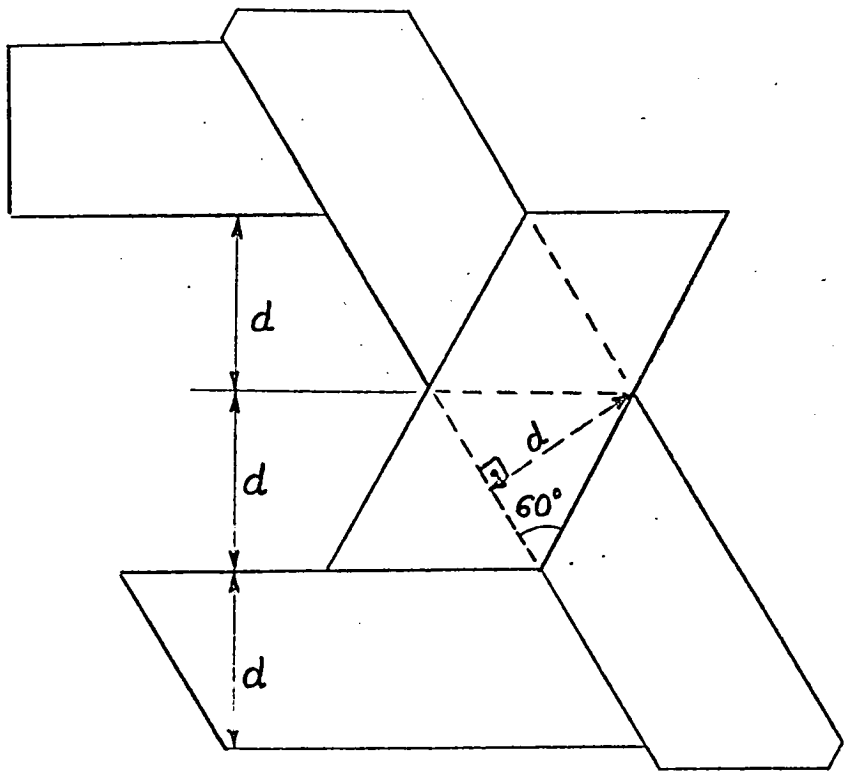

Fig. 4 Tri-directional weave - spacing

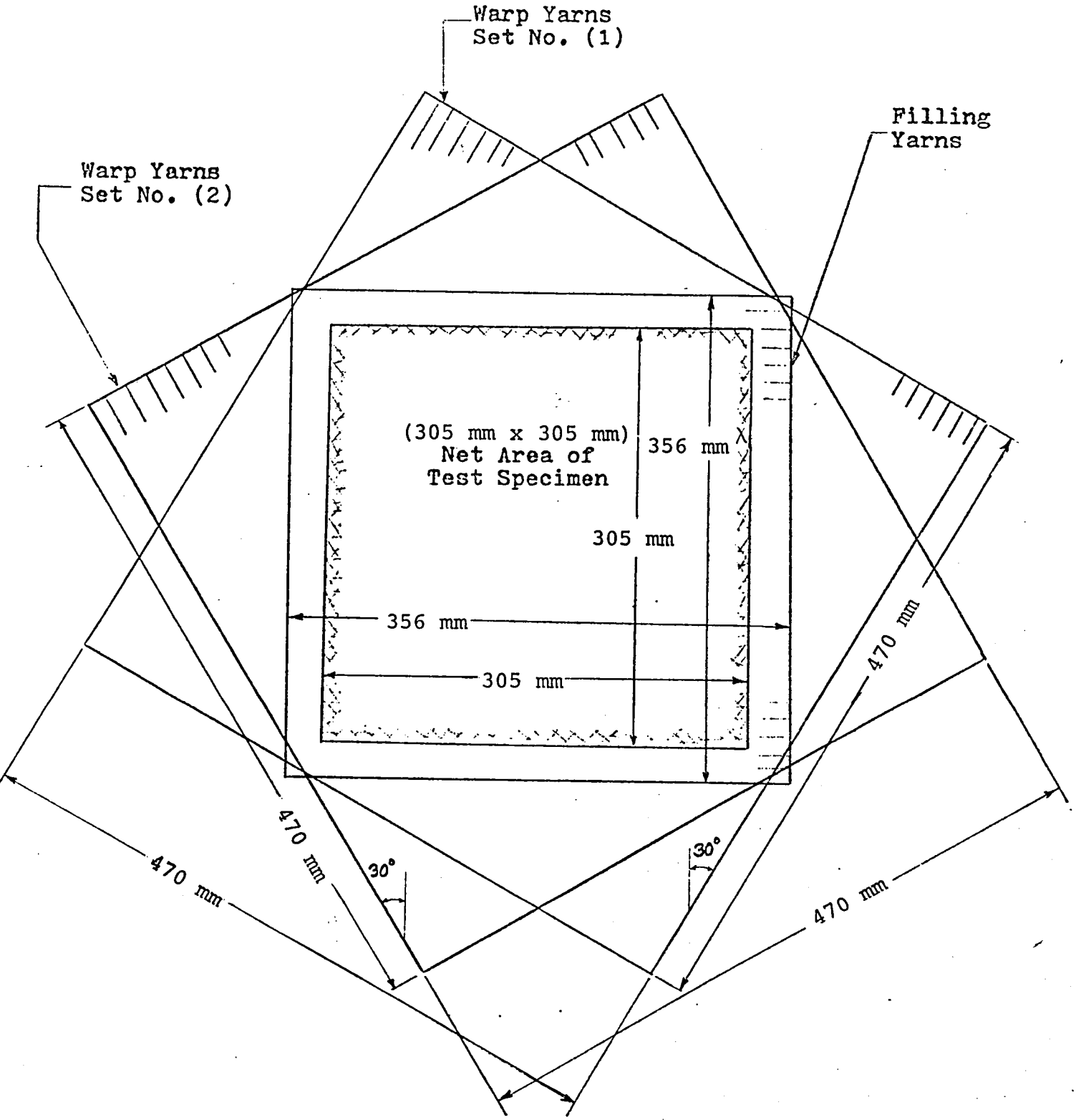

Fig. 5 Frame weaving of Tri-directional fabric

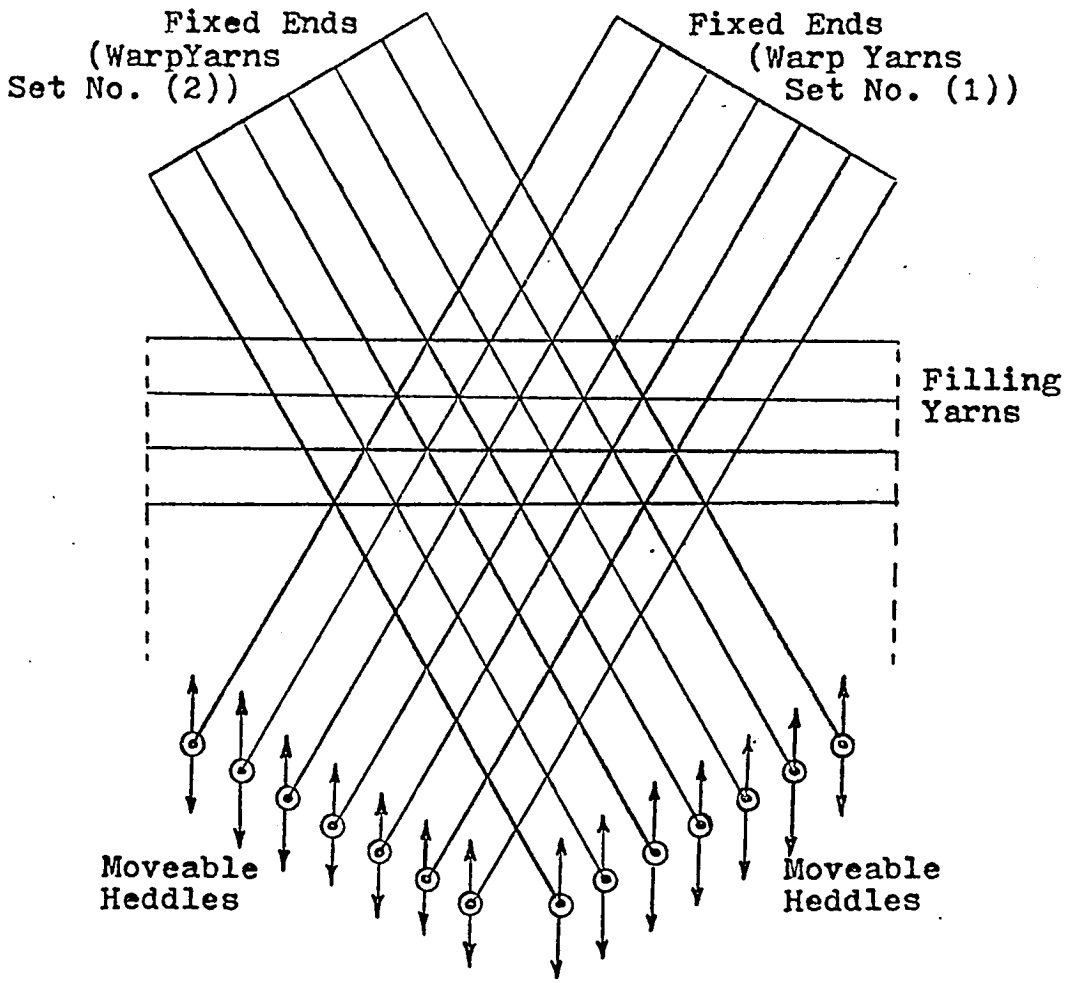

Fig. 6 Frame weaving of tri-directional fabric

Temperature - 440°-450° K

Pressure - 690 kPa

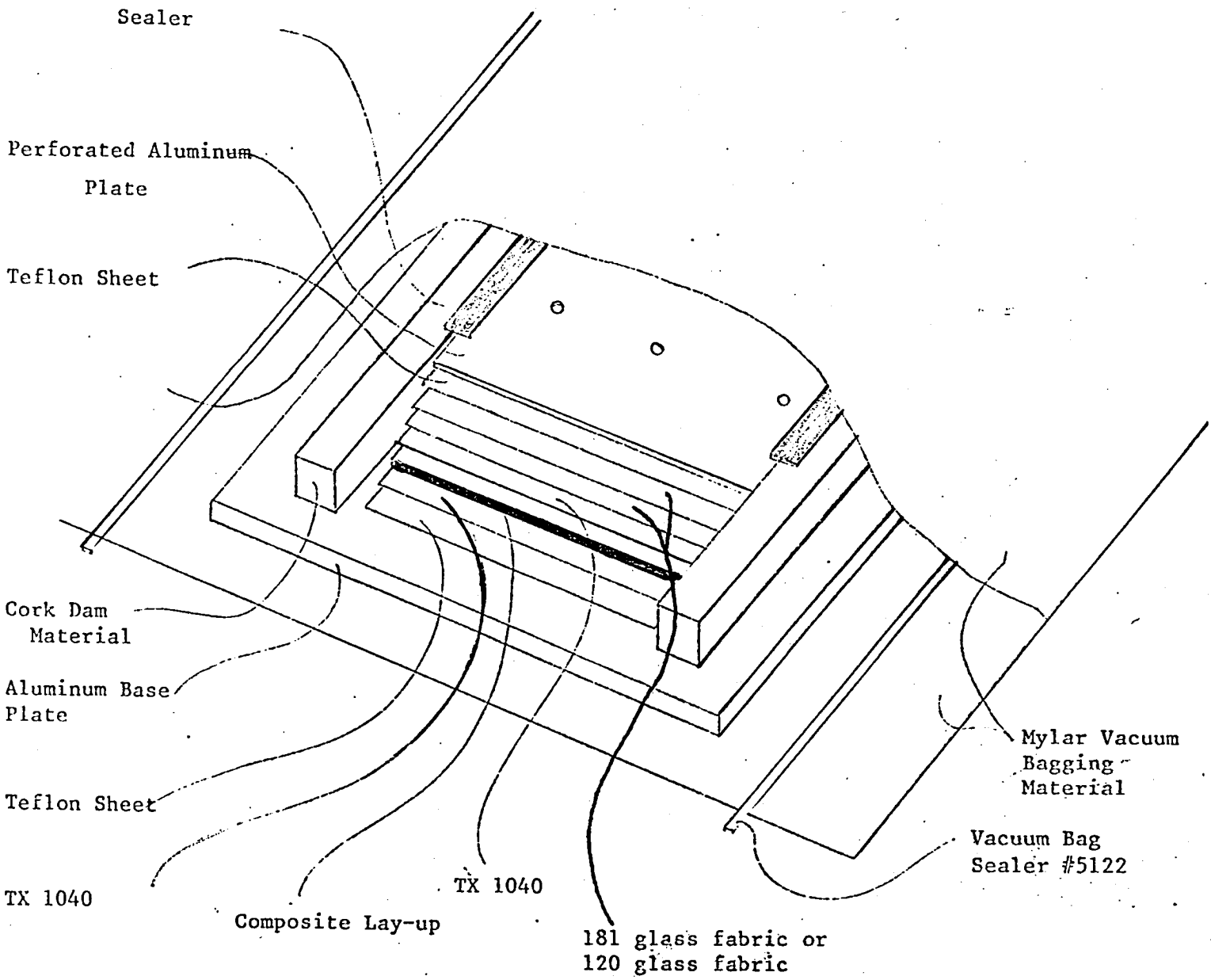

Fig. 7 Layering sequence

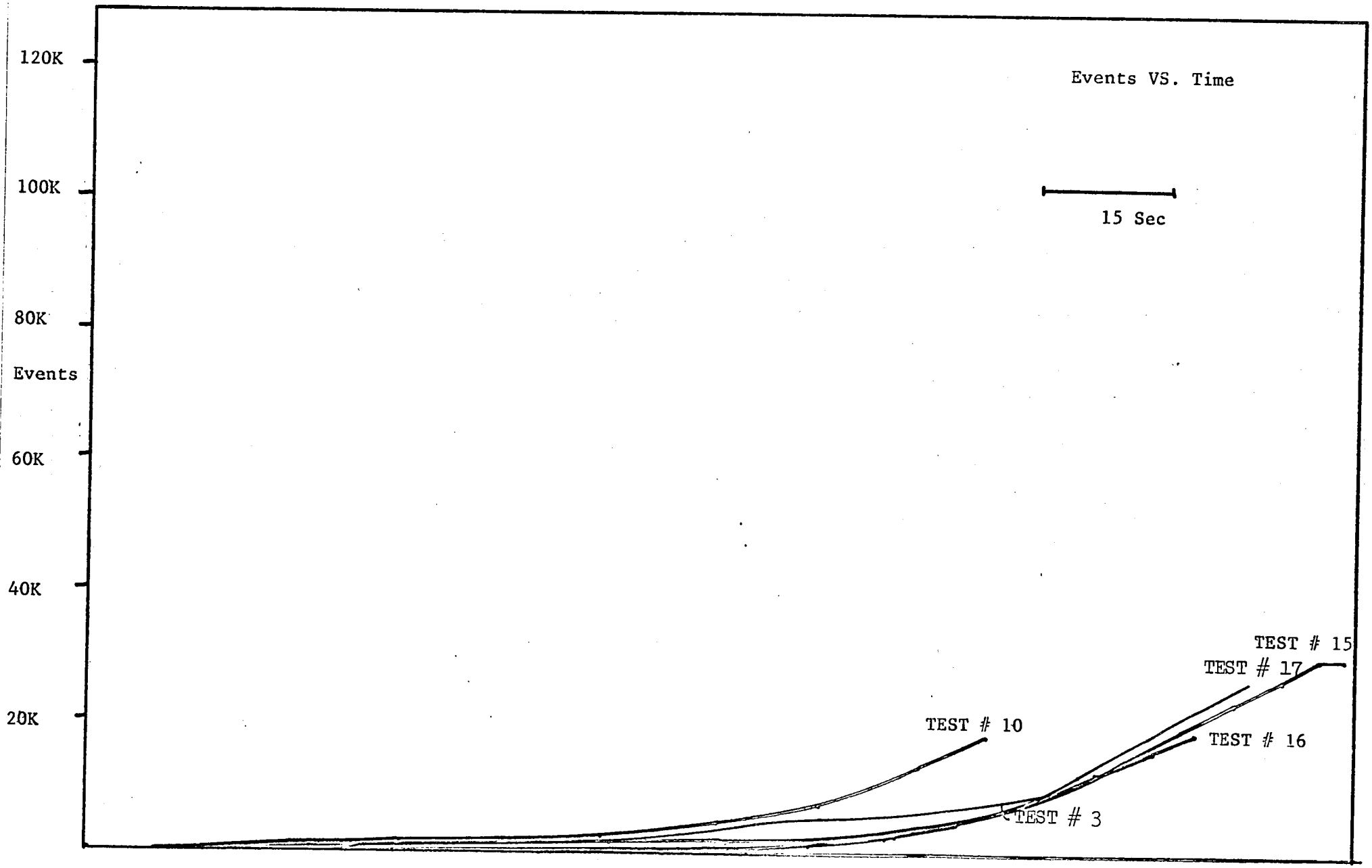

Fig. 8 Acoustic Emission events for 37% plain weave composite

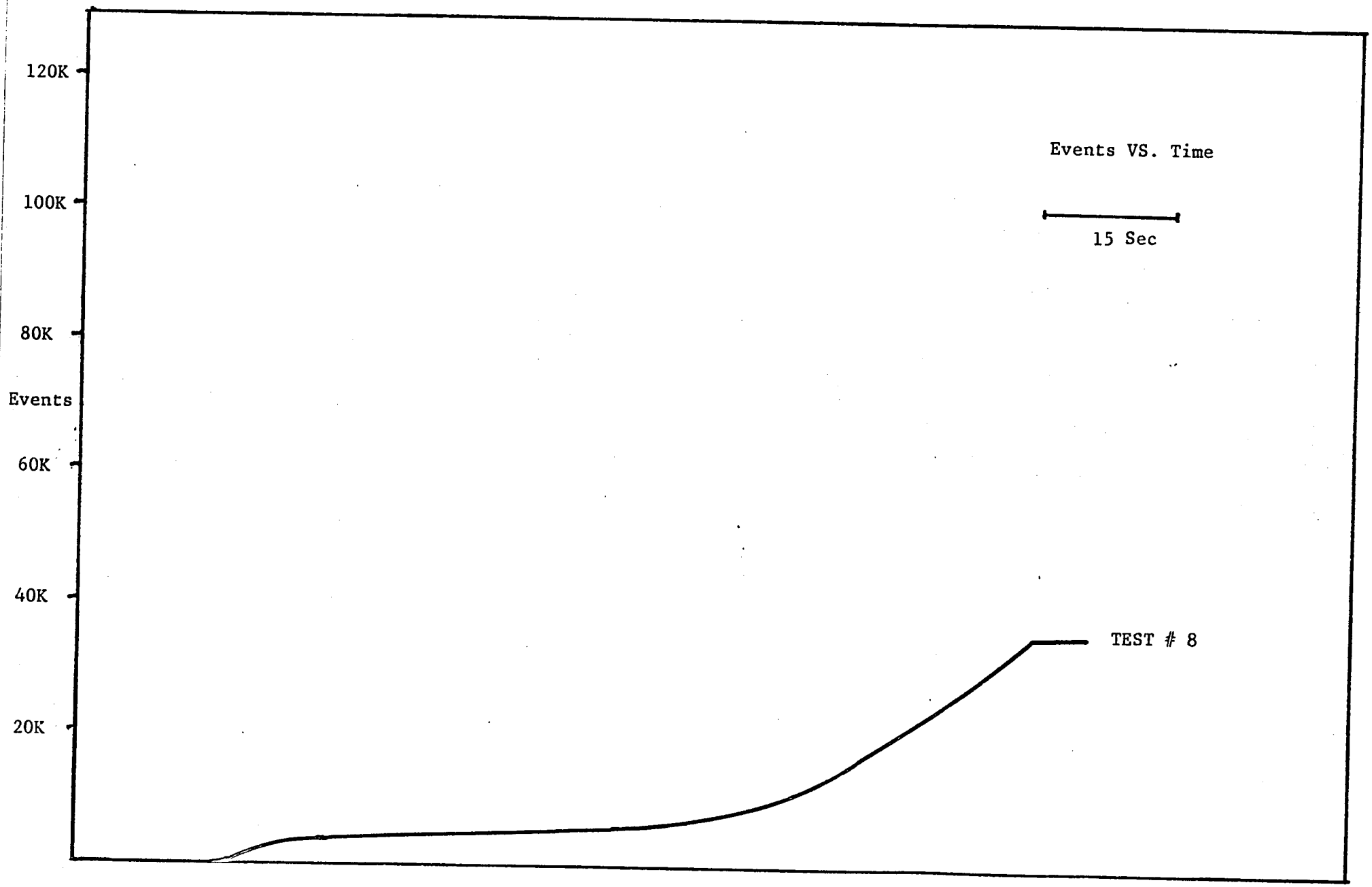

Fig. 9 Acoustic emission events for 22% plain weave composite

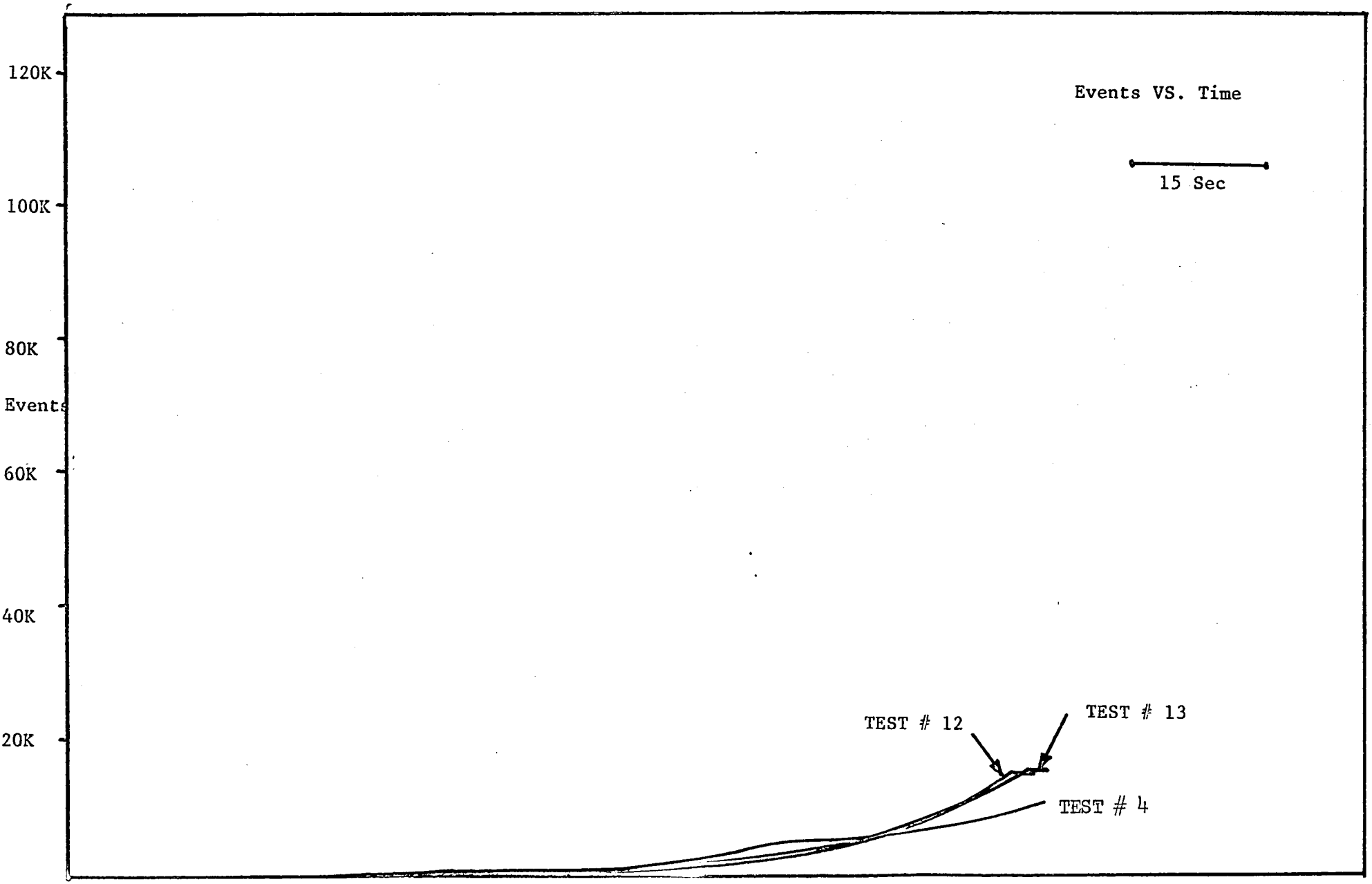

Fig. 10 Acoustic emission events for 50% plain weave composite

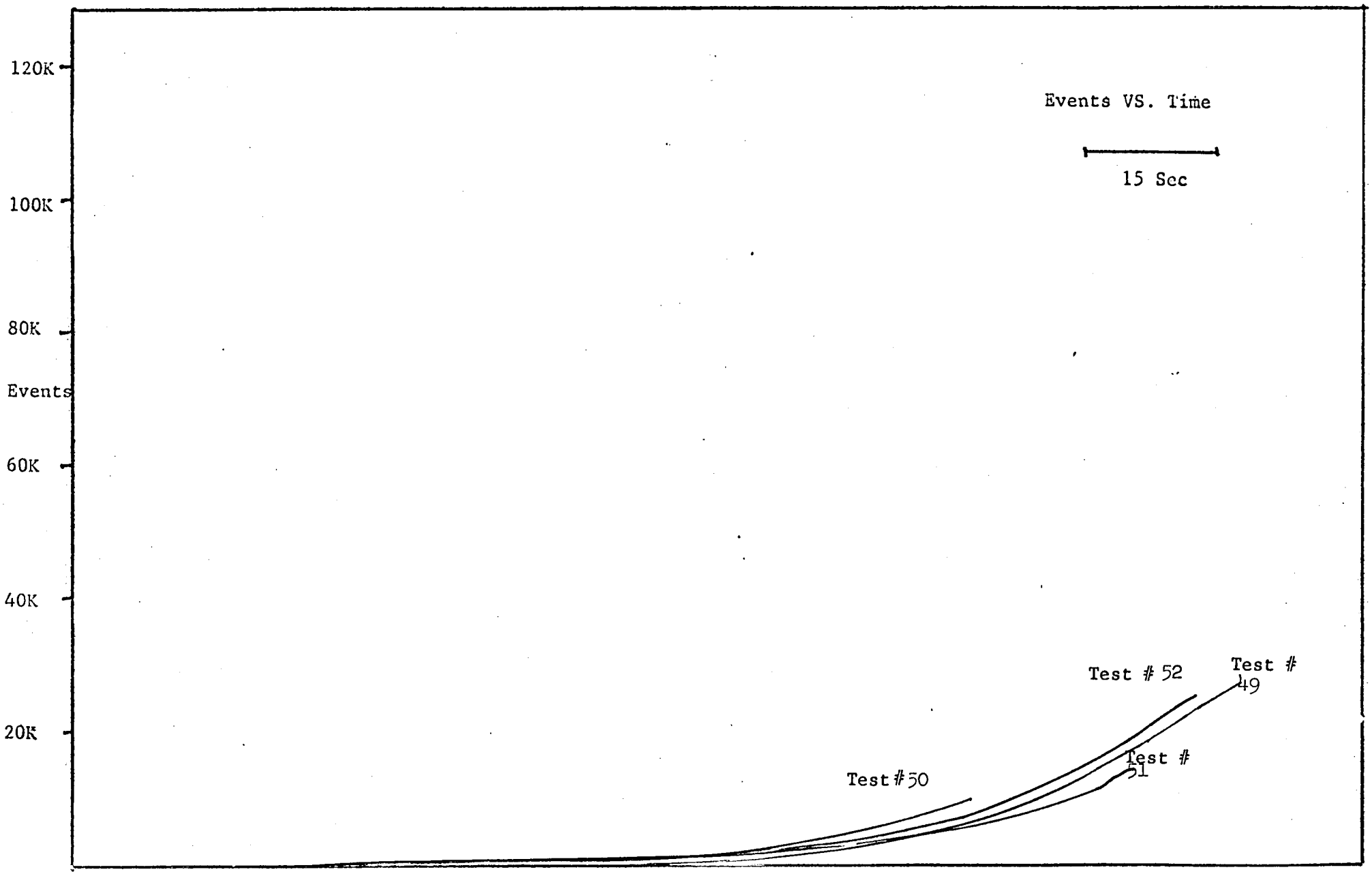

Fig. 11 Acoustic emission events for composite of tri-directional weave

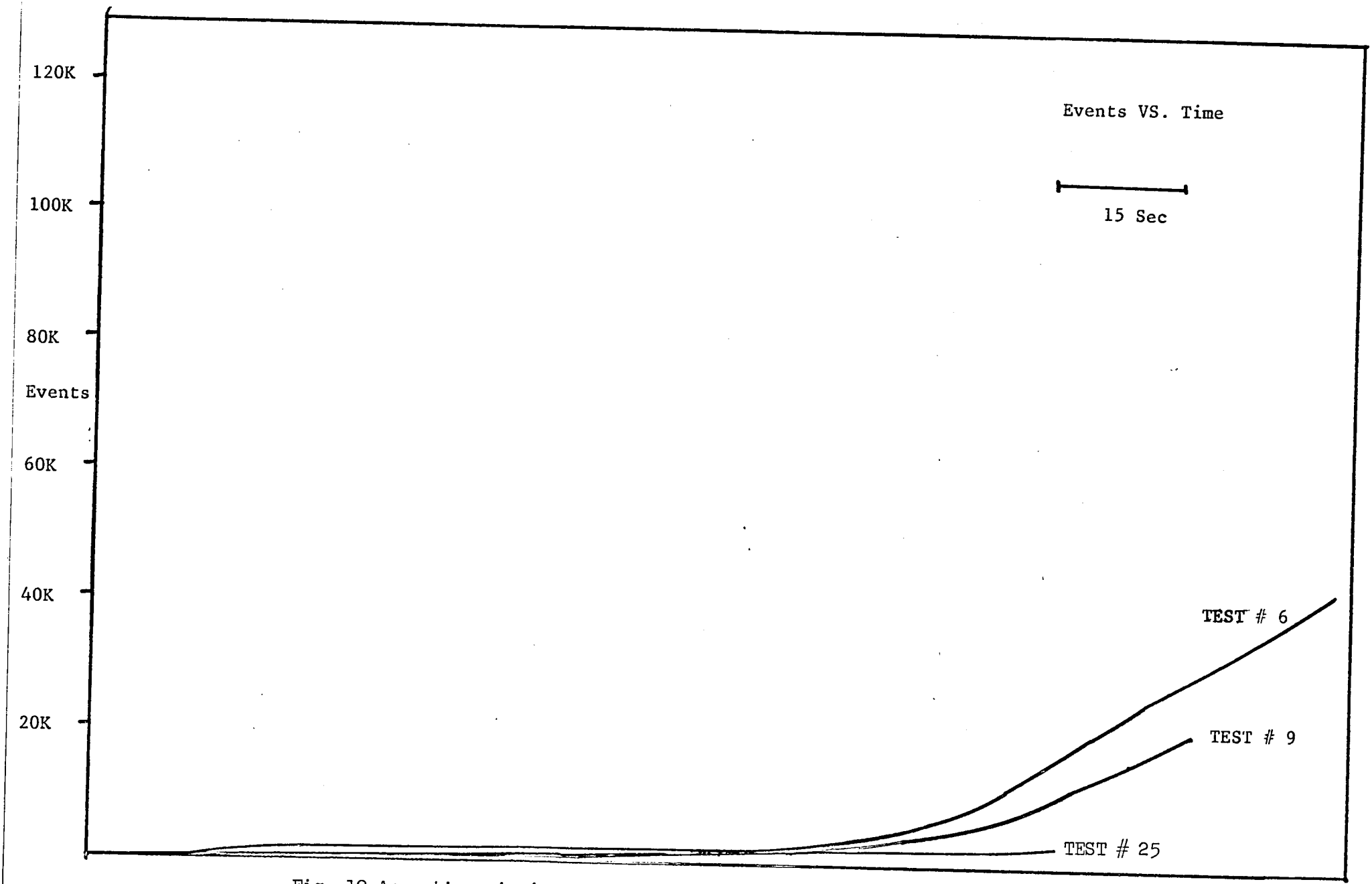

Fig. 12 Acoustic emission events from 37% unidirectional composite

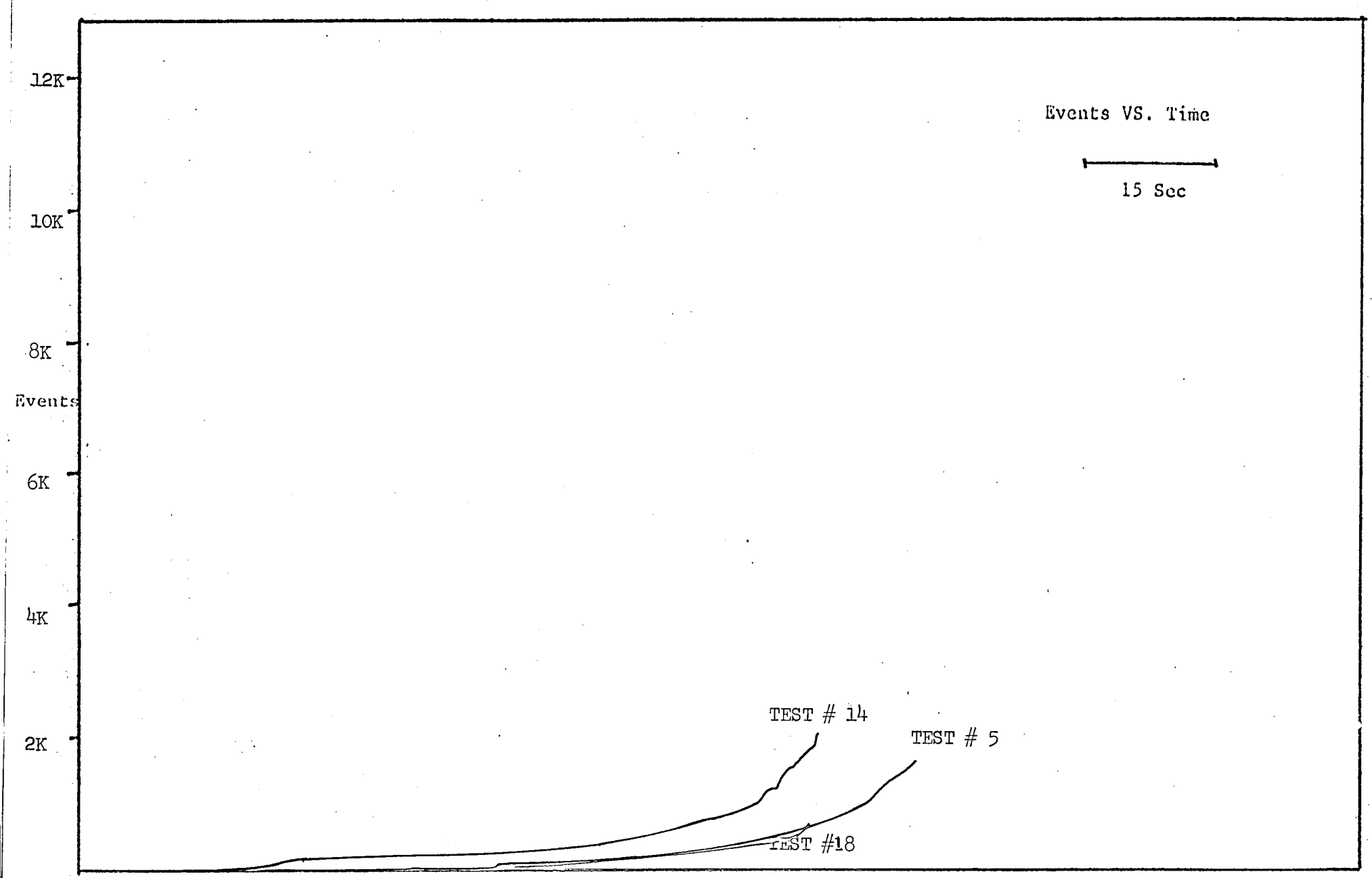

Fig. 13 Acoustic emission events for 50% unidirectional composites

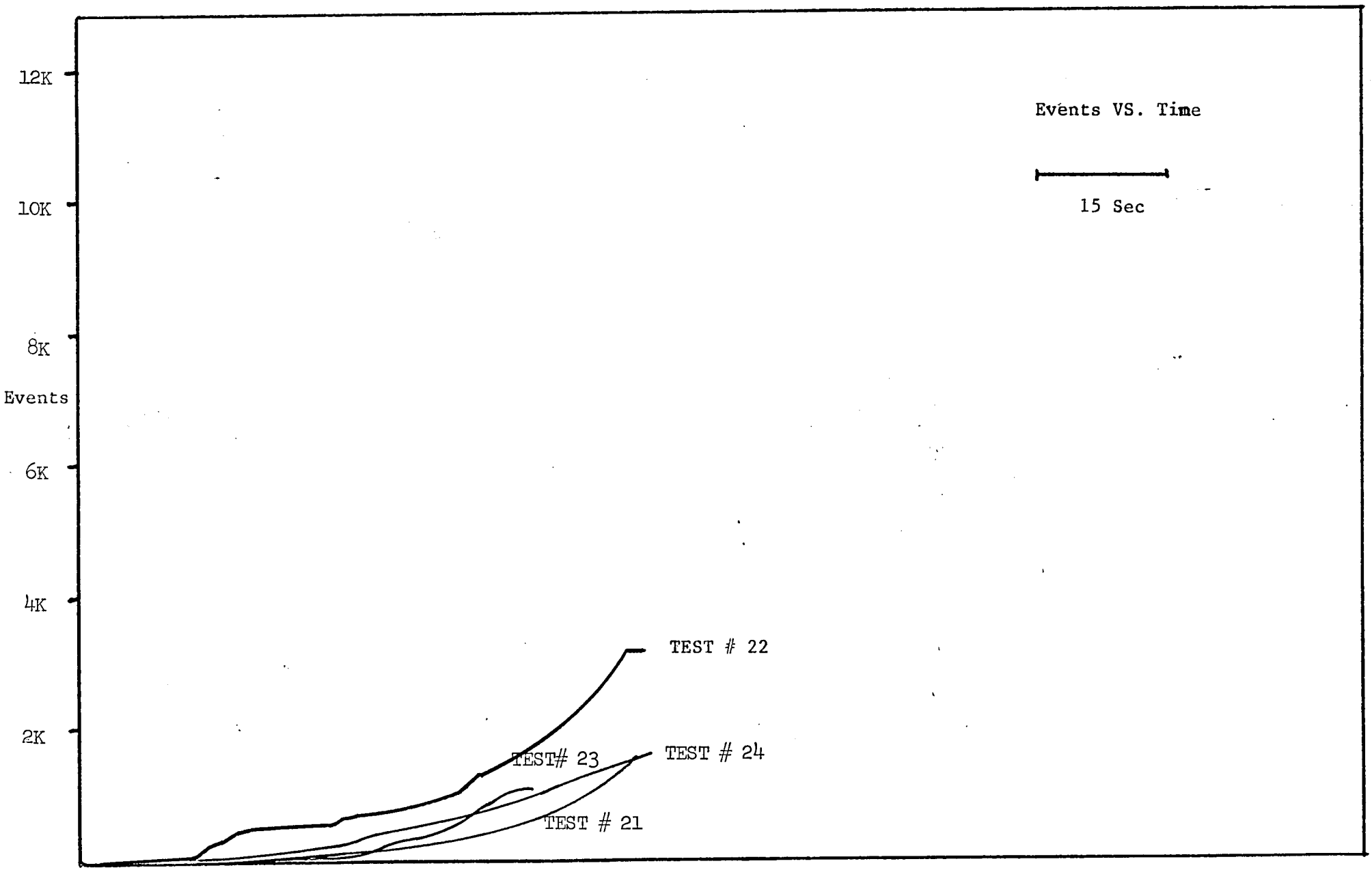

Fig. 14 Acoustic emission events for composite with holes

Fig. 15 Fractograph at 60 X

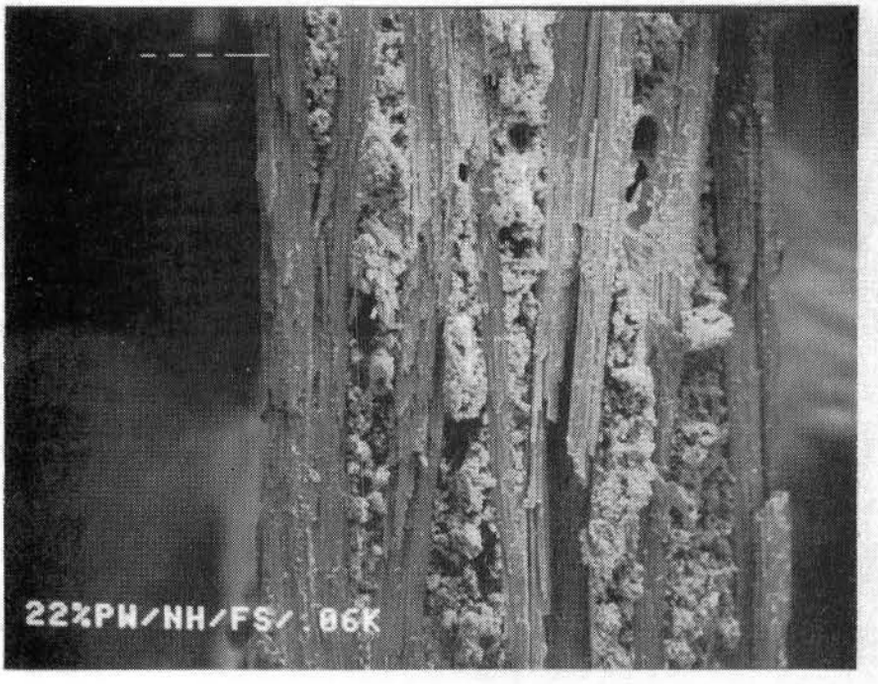

Fig. 16 Fractograph at 60 X

Fig. 17 Fractograph at 70 X

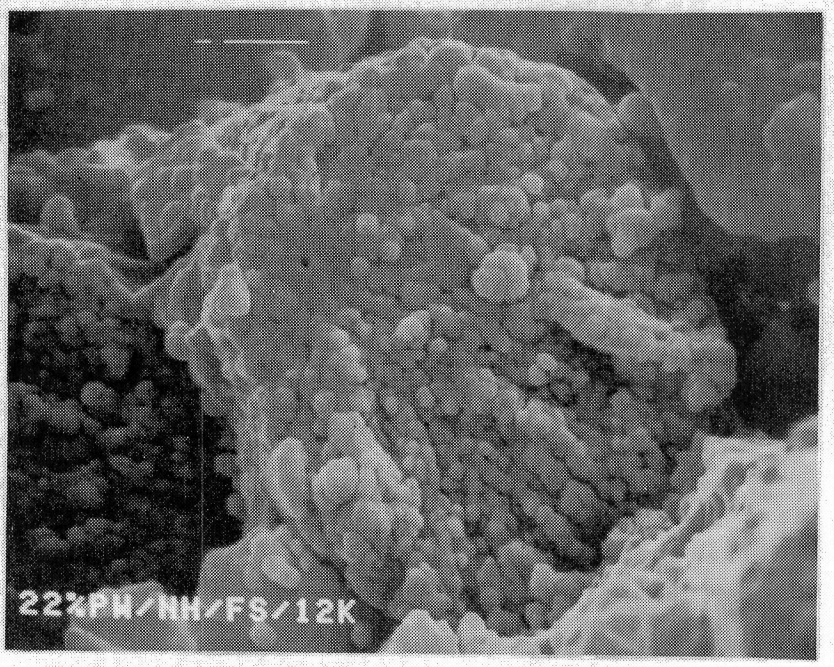

Fig. 18. Fractograph at 12000 X

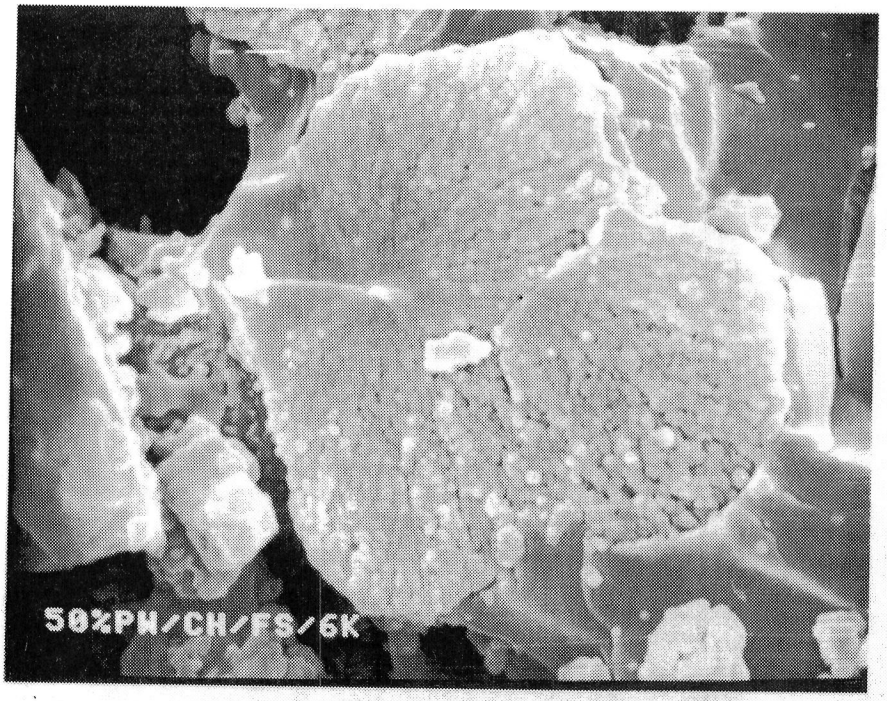

Fig. 19 Fractograph at 6000 X

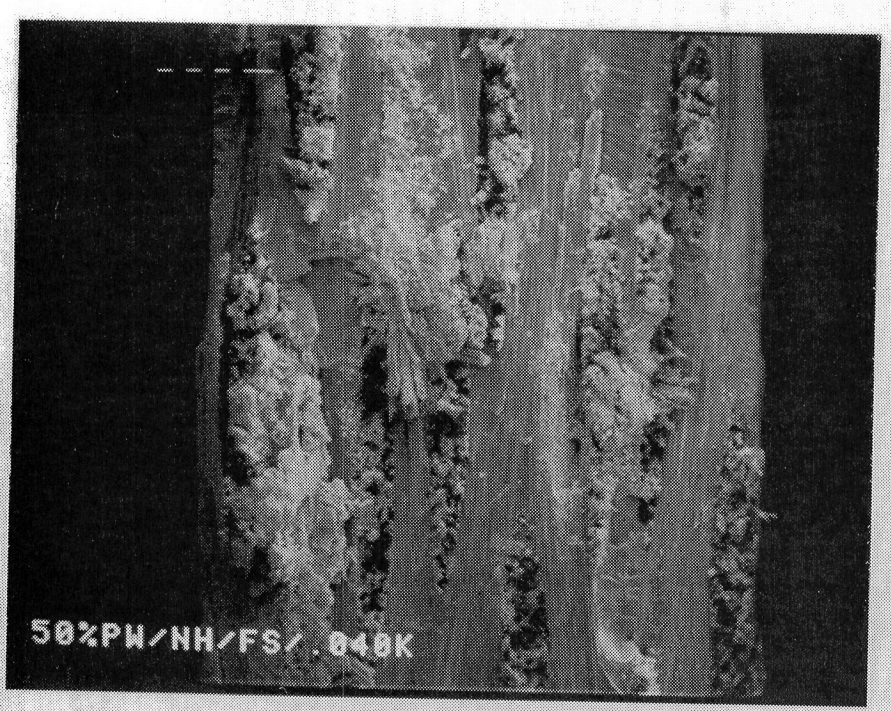

Fig. 20 Fractograph at 40 X

Fig. 21 Fractograph at 40 X

Fig. 22 Fractograph at 37 X

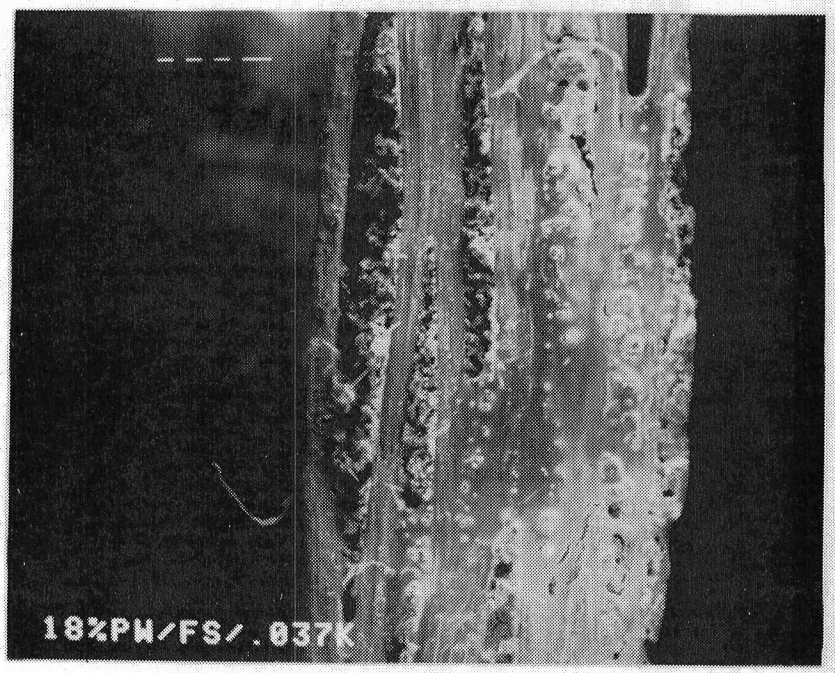

Fig. 23 Fractograph at 37 X

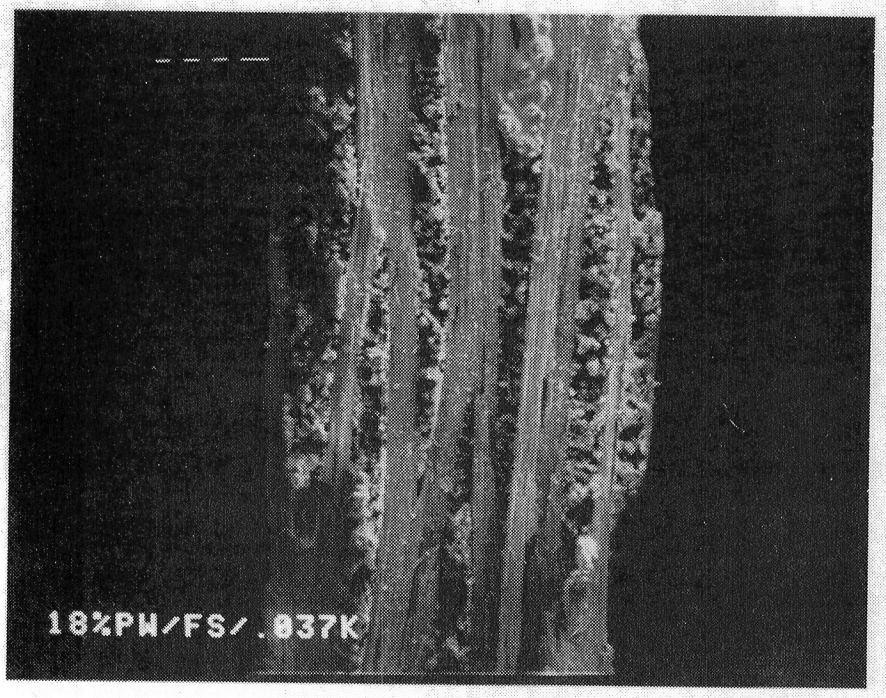

Fig. 24 Fractograph at 37 X

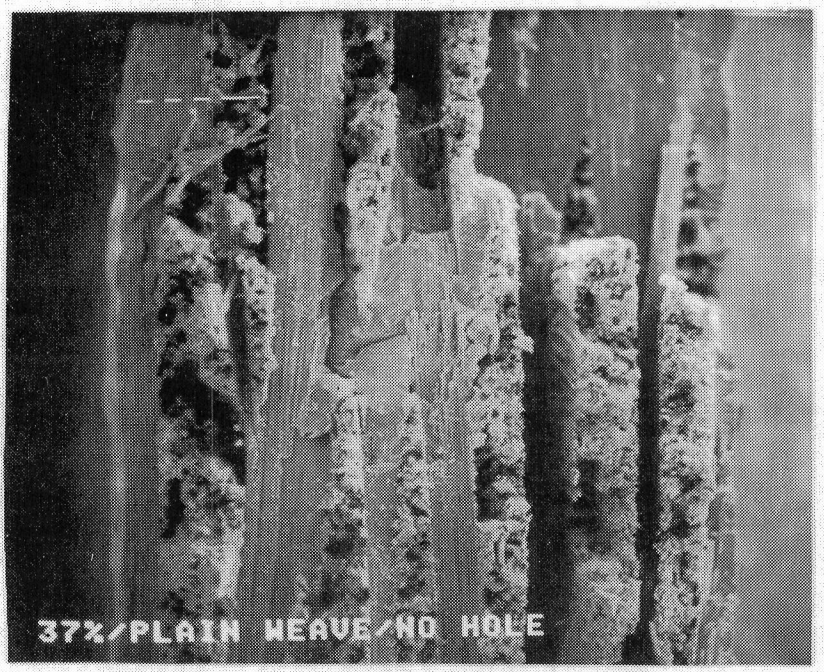

Fig. 24a Fractograph

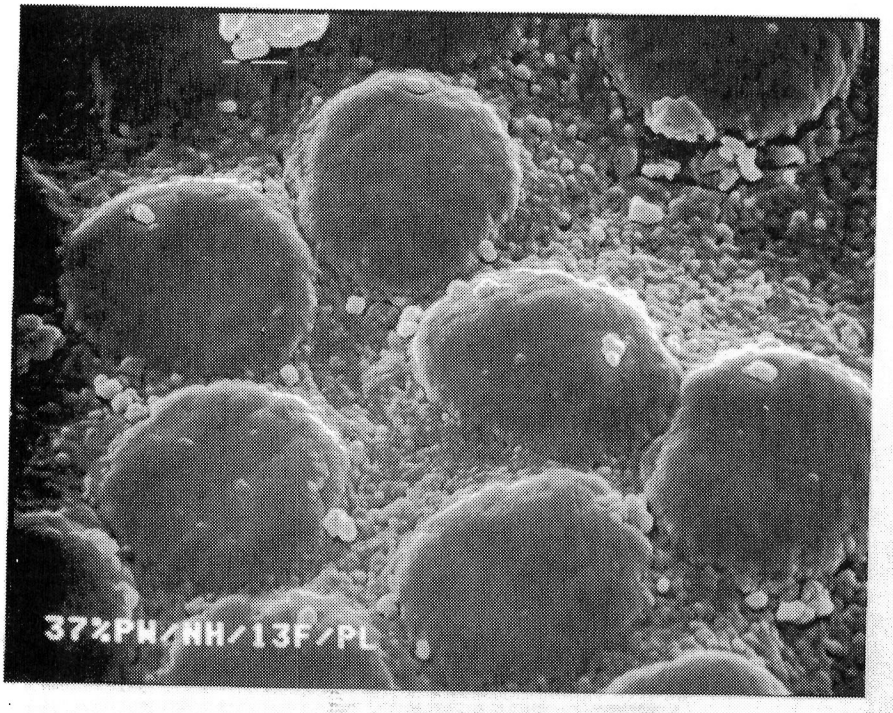

Fig. 25 Photomicrograph at 4700 X

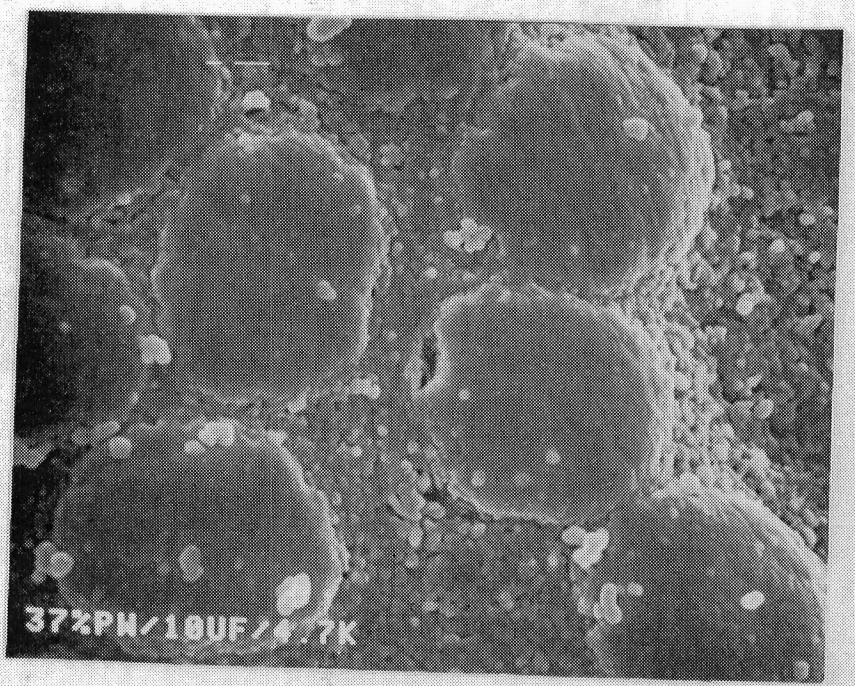

Fig. 26 Photomicrograph at 4700 X

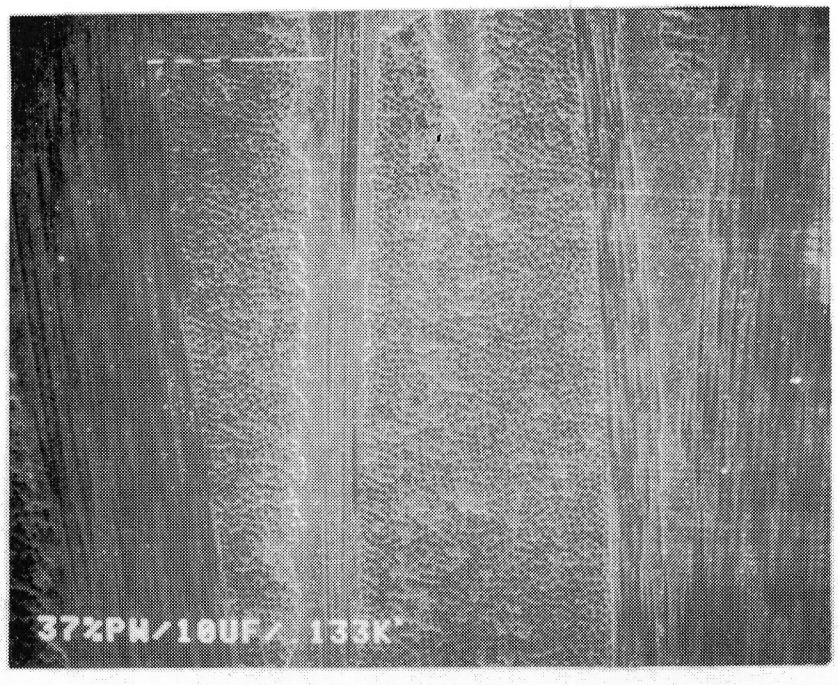

Fig. 27 Photomicrograph at 133 X

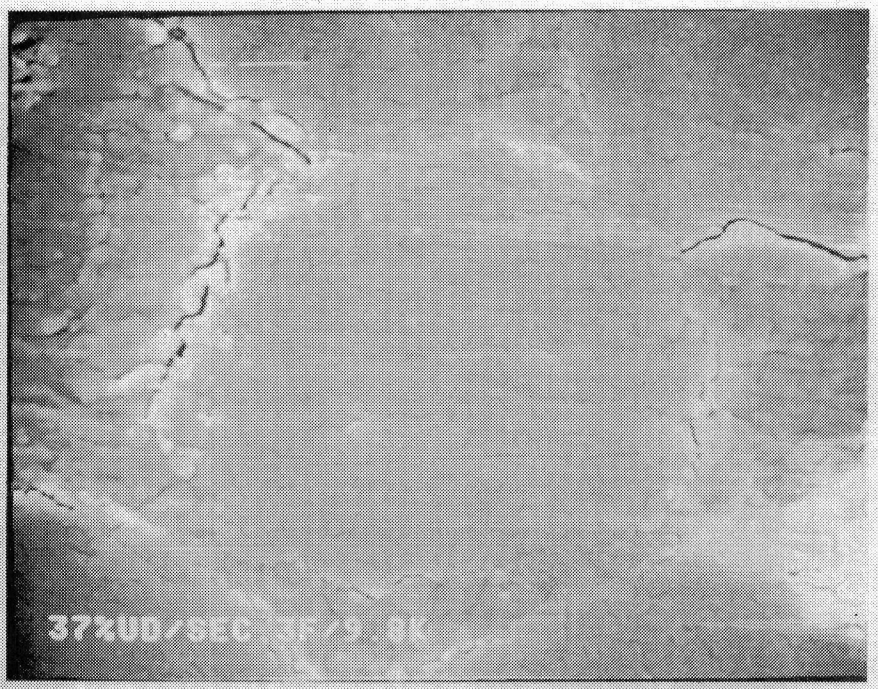

Fig. 28 Photomicrograph 9800 X

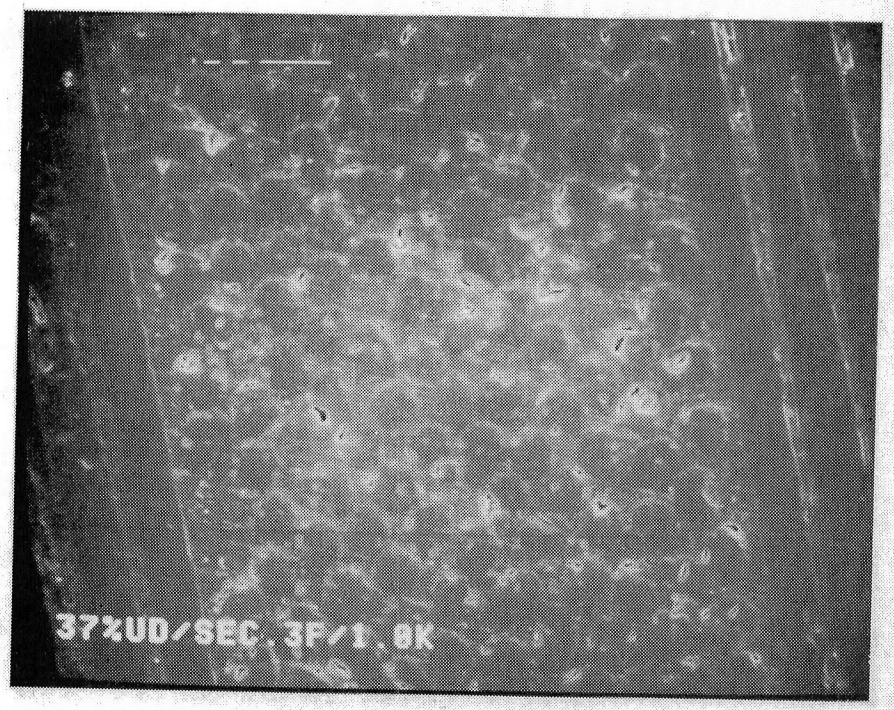

Fig. 29 Photomicrograph at 1000 X

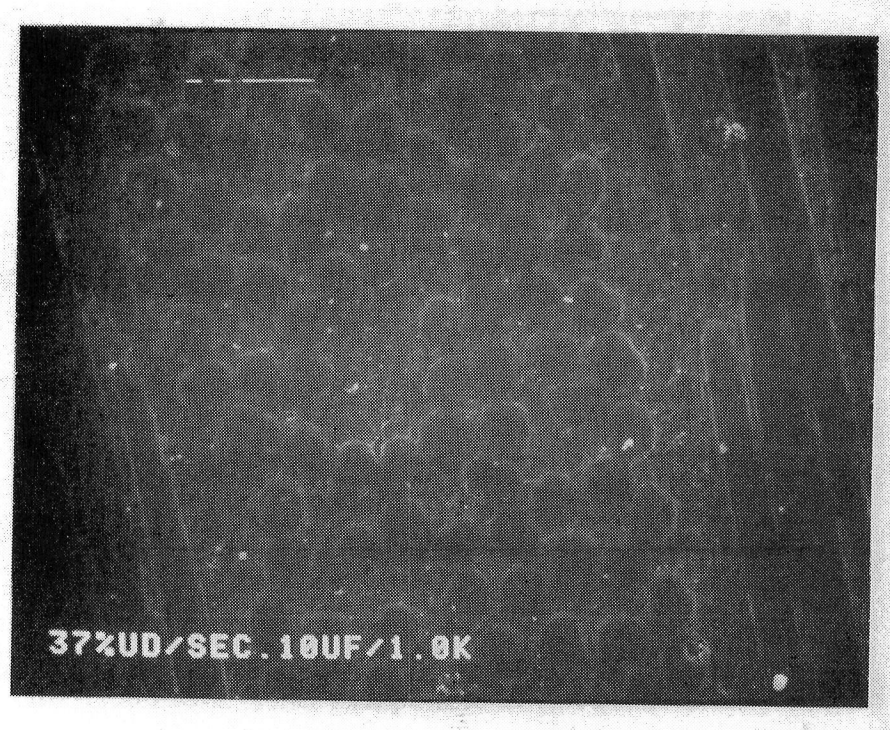

Fig. 30 Photomicrograph at 1000 X

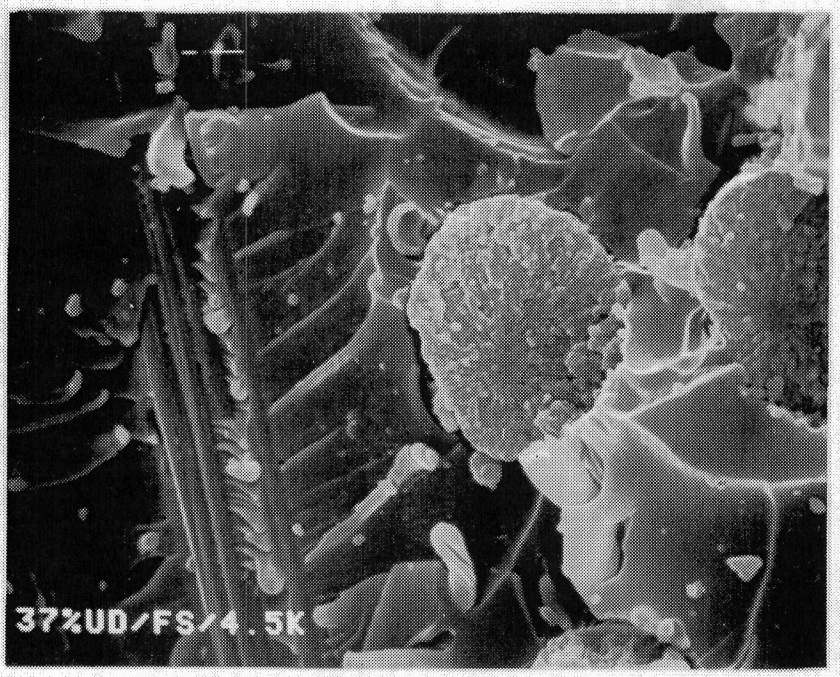

Fig. 31 Fractograph at 4500 X

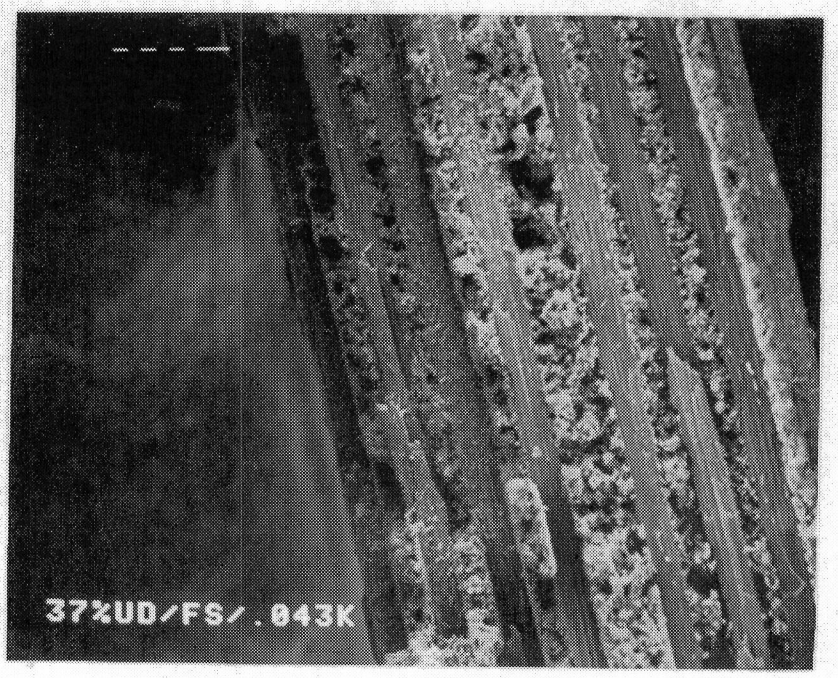

Fig. 32 Fractograph at 43 X

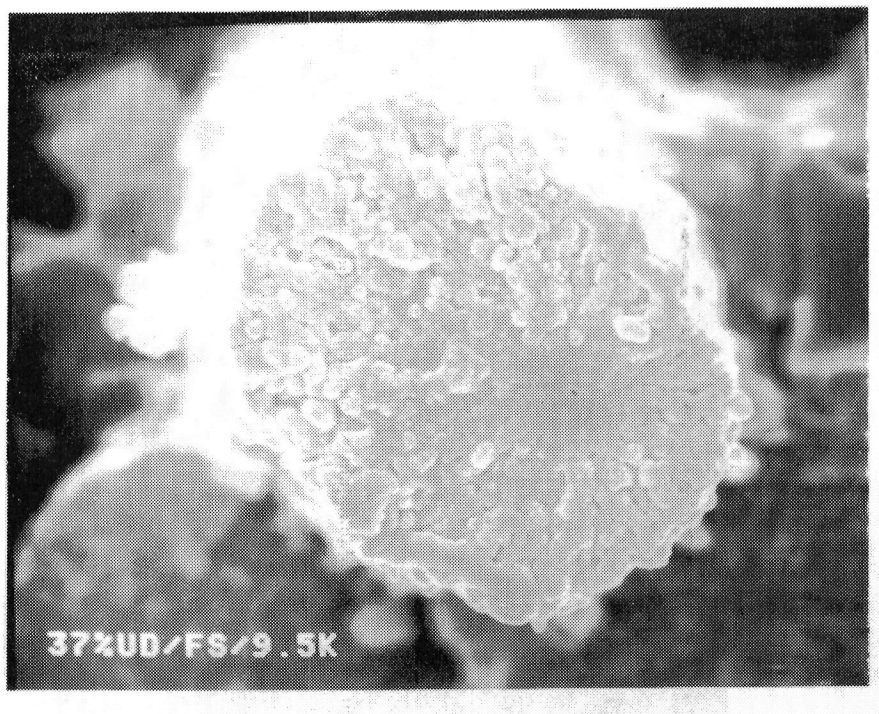

Fig. 33 Fractograph at 9500 X

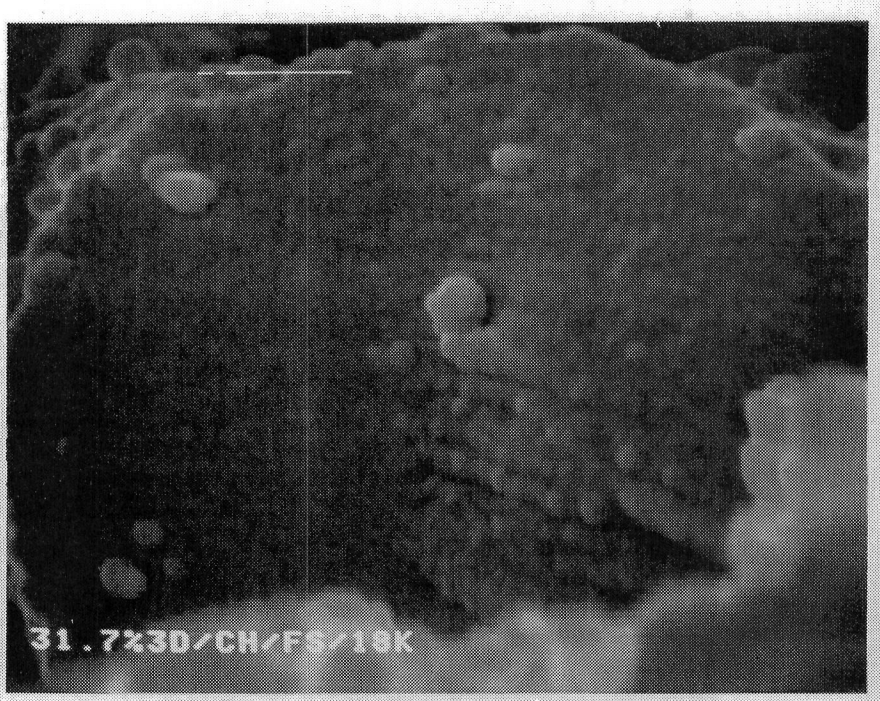

Fig. 34 Fractograph at 18000 X

Fig. 35 Fractograph at 12000 X

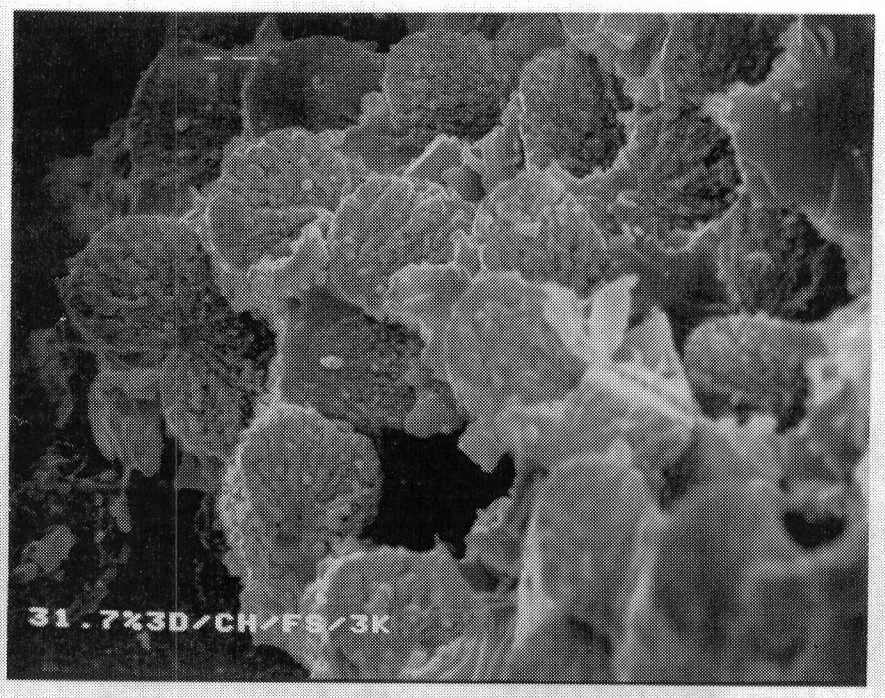

Fig. 36 Fractograph at 3000 X

Fig. 37 Fatigue Fractograph at 7000 X

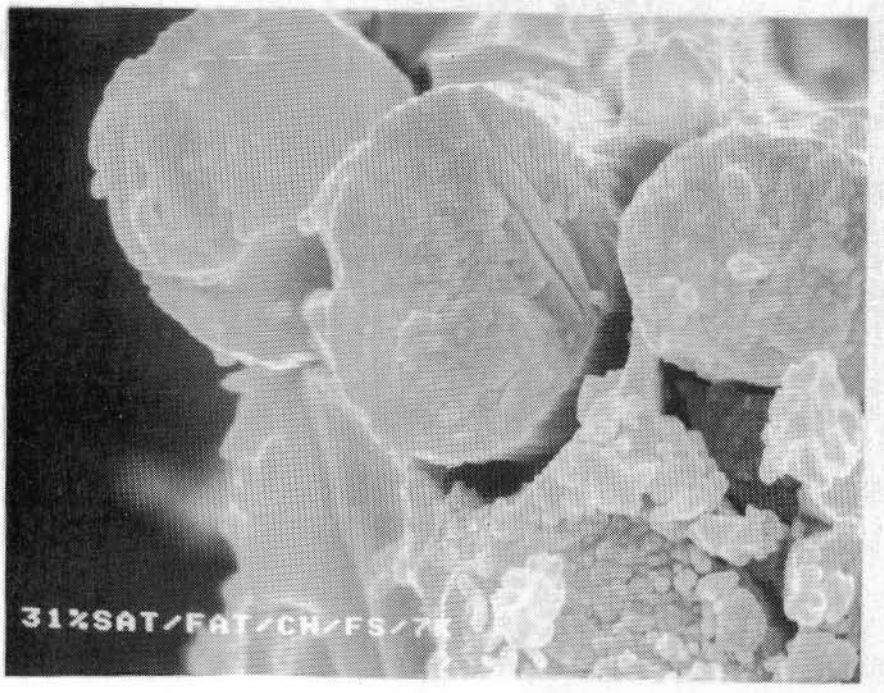

Fig. 38 Fatigue Fractograph at 7000 X

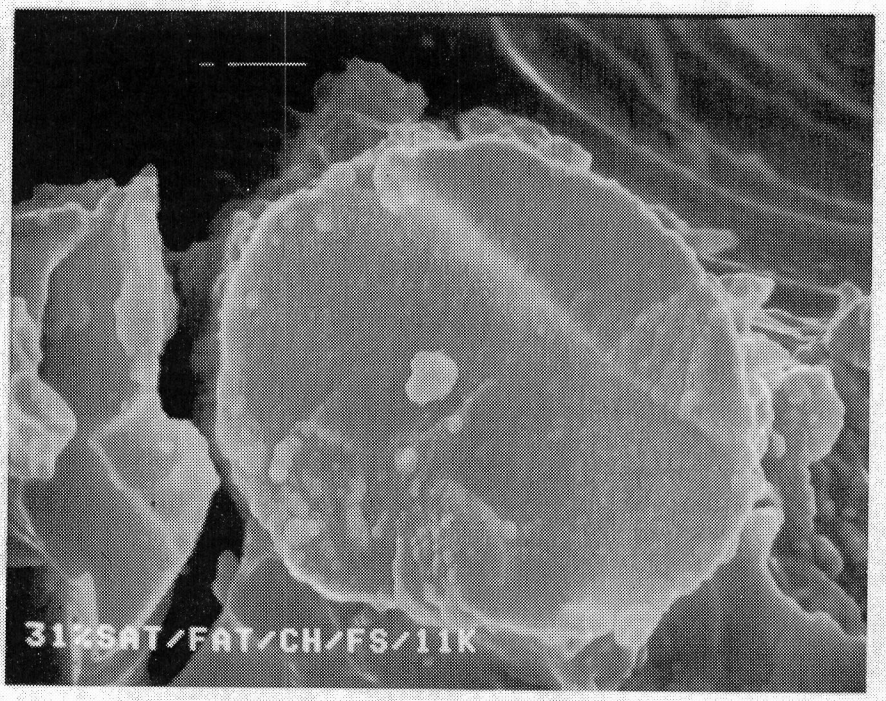

Fig. 39 Fatigue Fractograph at 11000 X

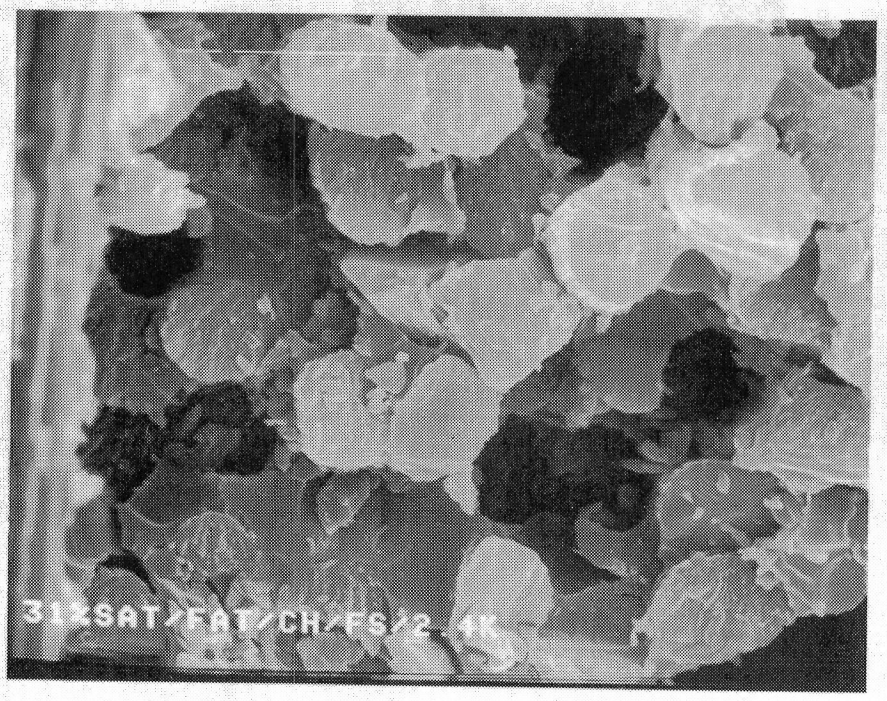

Fig. 40 Fatigue Fractograph at 2400 X

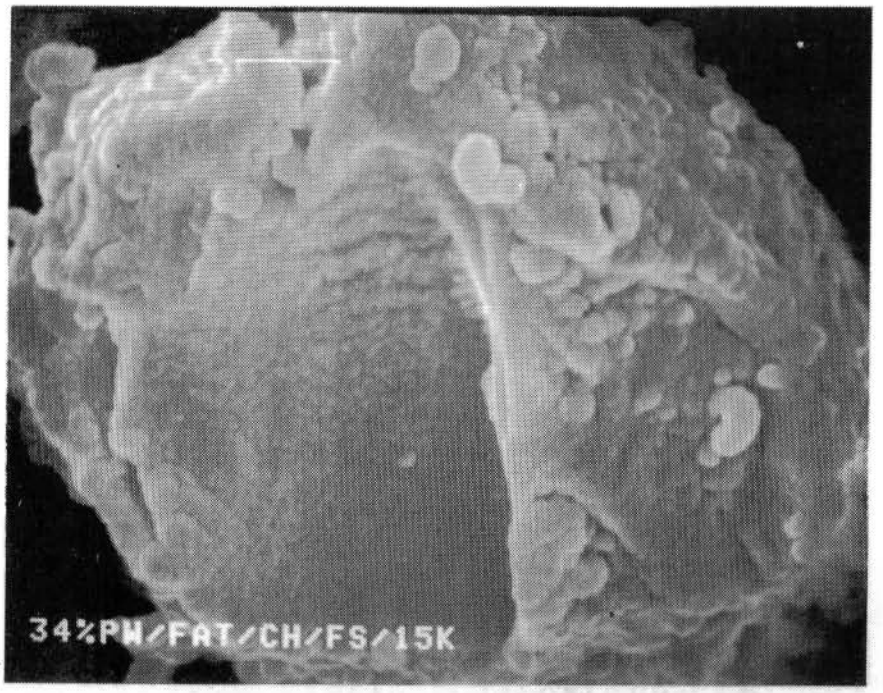

Fig. 41 Fatigue Fractograph at 15000 X

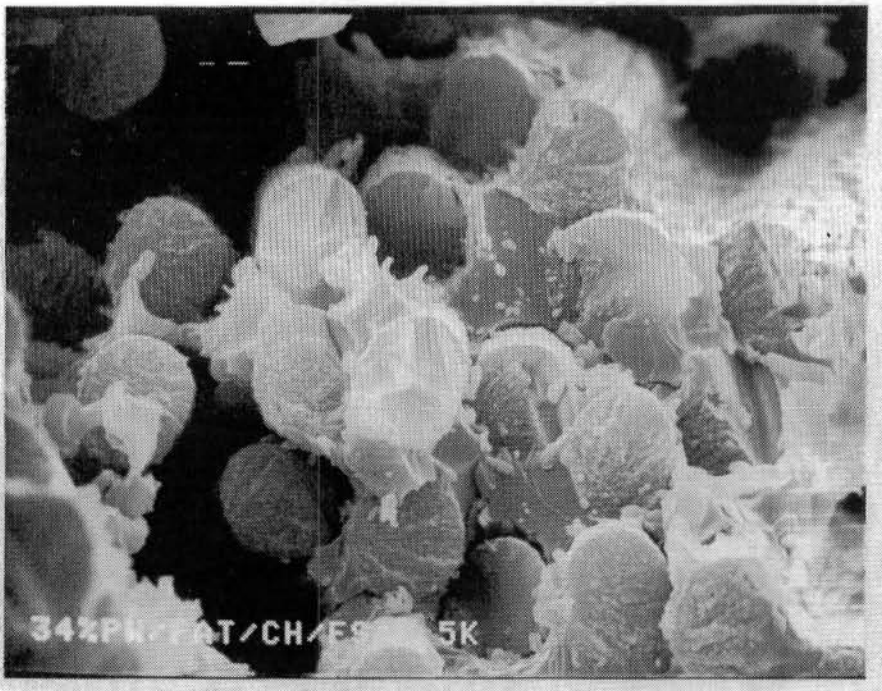

Fig. 42 Fatigue Fractograph at 2500 X

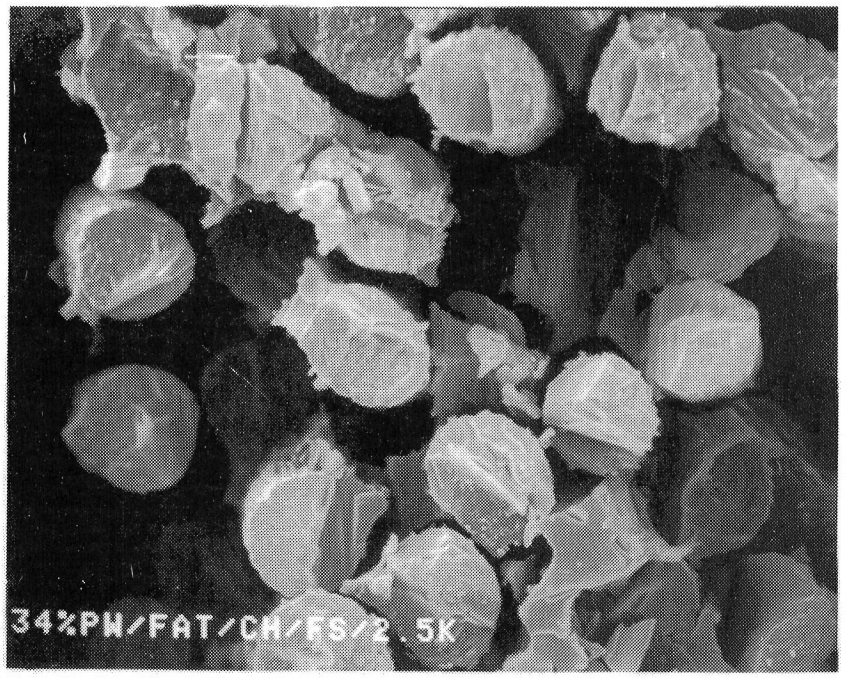

Fig. 43 Fatigue Fractograph at 10,000 X

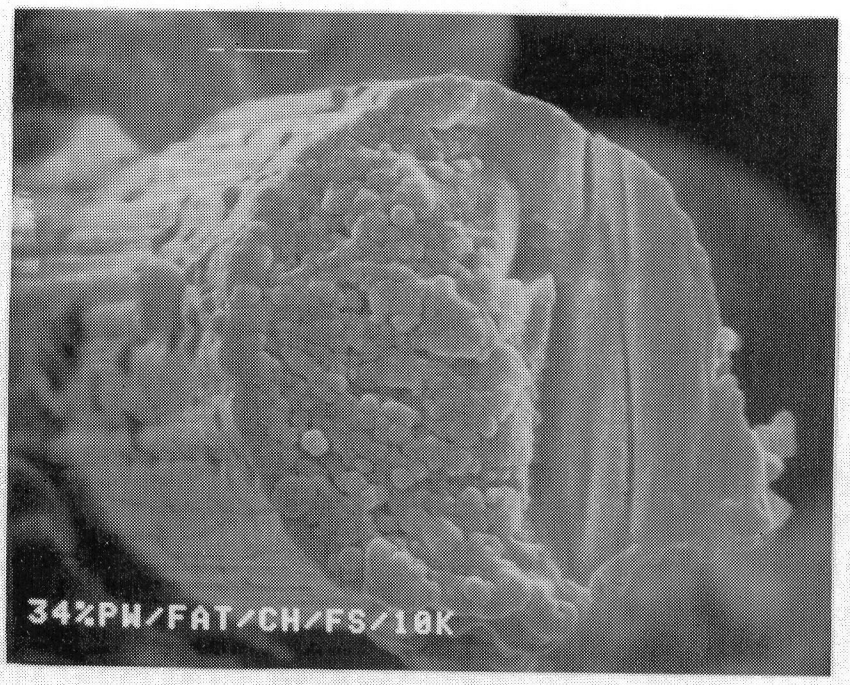

Fig. 44 Fatigue Fractograph at 2500 X